



Assessment of Bray Moss Libby formulation for premixed flame-wall interaction within turbulent boundary layers: Influence of flow configuration



Umair Ahmed^a, Nilanjan Chakraborty^a, Markus Klein^{b,*}

^a School of Engineering, Newcastle University, Newcastle upon Tyne NE1 7RU, United Kingdom

^b Department of Aerospace Engineering, Bundeswehr University Munich, Neubiberg, Germany

ARTICLE INFO

Article history:

Received 2 March 2021

Revised 19 June 2021

Accepted 20 June 2021

Keywords:

Flame-wall interaction

Turbulent channel flow

V-flame

Head-on quenching

Premixed turbulent combustion

Direct Numerical Simulation

ABSTRACT

Three-dimensional direct numerical simulations (DNS) of two different flow configurations have been performed for premixed flames interacting with chemically inert isothermal walls at the unburned gas temperature in fully developed turbulent boundary layers. The first configuration is an oblique flame-wall interaction (FWI) of a V-flame in a turbulent channel flow and the second configuration is a head-on quenching planar flame in a turbulent boundary layer. These simulations are representative of stoichiometric methane-air mixture at unity Lewis number under atmospheric conditions. The turbulence in the non-reacting conditions for these simulations is representative of the friction velocity based Reynolds number of $Re_\tau = 110$. Differences in the statistical behaviours of the mean values of progress variable, temperature, and density during the FWI process have been reported for the two configurations. It is found that the mean flame brush thickens in the near wall region leading to significant departures from the strict Bray Moss Libby (BML) formulation limit during the FWI process and that is reflected in the probability density function (PDF) distributions of c for both flame configurations. The closures from the BML formulation for Reynolds averaged progress variable \bar{c} and the Favre averaged variance of the progress variable $\tilde{c}^{1/2}$ have also been investigated and it is found that these closures need to be modified to account for the FWI process even when the flame away from the wall represents high Damköhler number premixed turbulent combustion. Furthermore, the statistical behaviours of the quantities required for Flame Surface Density (FSD) based mean reaction rate closure including the flame orientation factor σ_y , the flamelet length scale L_y and the flame stretch factor I_0 have been interrogated from the DNS data for the two flame configurations. The flamelet length scale and the stretch factor extracted from the DNS data are compared with the closures for these quantities proposed in the literature. It is found that σ_y exhibits significant spatial variation for both cases. The existing closures for L_y and I_0 which exhibit the best quantitative agreement with DNS data have been identified. It has been found that the models for L_y and I_0 have scopes for further improvement to enable satisfactory predictions of these quantities during the FWI process within turbulent boundary layers.

© 2021 The Combustion Institute. Published by Elsevier Inc. All rights reserved.

1. Introduction

Reduction in greenhouse gases and the control of pollutant emissions are becoming increasingly important for the power generation, automotive and aviation industry. As a consequence the combustors are being made more fuel efficient and smaller in size to increase energy density thus leading to events like flame-wall interaction (FWI) within the combustion chamber. This phenomena occurs in many engineering devices (e.g. spark ignition (SI)

engines, gas turbines and micro-combustors), and its modelling remains challenging. During these events combustion is strongly affected by the presence of walls, which leads to flame quenching due to wall heat losses. The flame also has a significant effect on the flow near the wall as well as on the heat flux to the wall [1]. Under these conditions, the turbulence structure is altered by the presence of walls and the interaction of flame elements with walls leads to modifications of the underlying combustion processes [2]. In practice, limited information is available regarding the behaviour of turbulence and combustion processes during FWI in fully developed boundary layers and consequently there is a lack of modelling strategies available in the literature.

* Corresponding author.

E-mail address: markus.klein@unibw.de (M. Klein).

There are several numerical and experimental studies which focus on the issues related to FWI for premixed combustion in different flame or flow configurations. Head-on quenching of premixed turbulent flames under isotropic turbulence conditions has been investigated using two dimensional Direct Numerical Simulation (DNS) data by Poinsot et al. [3], and by Chakraborty and co-workers [4–10] using three-dimensional DNS data for both unity and non-unity Lewis number premixed flames. In these numerical studies, there is no mean flow and the flame propagates towards the wall and is eventually quenched in the vicinity of the cold wall. In these simulations, turbulence decays rapidly during the FWI process and cannot easily be quantified, but these simulations still provide important physical insights into quenching distances and the influence of chemistry in FWI. The limitations of the aforementioned simulations related to the quantification of turbulence in FWI can be overcome by investigating fully developed turbulence in boundary layers. Such simulations have been performed via DNS by Bruneaux et al. [11,12] in a constant density turbulent channel flow and this work has been extended by Alshaalan and Rutland [1,2] by performing a premixed V-flame simulation in a turbulent channel-Couette flow. These studies demonstrate that the near-wall structures have a strong influence on the flame when it is in the vicinity of the wall. In this case the flame is pushed towards the wall by turbulent structures leading to higher wall heat fluxes and localised flame quenching. At the same time the vortical structures transport unburned fluid away from the wall and carry it into the burned gases, consequently creating pockets of fresh gases in the burnt gas regions. The work on FWI within turbulent channel flows with isothermal inert walls has been extended by Gruber et al. [13] and Ahmed et al. [14] in the case of a premixed V-flame, and by Gruber et al. [15,16], Kitano et al. [17] and Ahmed et al. [18,19] in the case of turbulent boundary layer flashback. More recently, FWI has also been investigated under adiabatic wall boundary conditions by Ahmed et al. [14] for a premixed V-flame configuration within turbulent channel flows. The physical phenomenon in the near wall region during FWI has also been investigated in statistically planar turbulent premixed flames impinging on a flat inert wall at different temperatures by Zhao et al. [20–22] and for different fuel Lewis numbers by Konstantinou et al. [23]. Recent experimental findings for V-flames interacting with cold walls [24–26] and transient head-on quenching [27] have confirmed the DNS findings regarding the influence of the flame on turbulence and vice versa. All of the aforementioned numerical and experimental studies show that the flame front has a strong influence on the approaching turbulence and at the same time the turbulence significantly affects the flame structure.

In the case of premixed turbulent combustion, accurate prediction of FWI events and the resulting heat loss for industrial combustion processes using computational methods remains a challenge, and usually requires the use of statistical methods. In many cases, the total aerothermochemistry of the flow can be described by a Probability Density Function (PDF) and a multidimensional PDF can in principle be obtained by a PDF transport equation [28,29]. This procedure circumvents a number of modelling assumptions and consequently produces a general mean reaction rate closure. However, the method requires a closure for the molecular diffusion terms which remains a modelling challenge [29]. In the high Damköhler number limit, the modelling can be simplified under the thin flamelet assumption. In this approach, the flame is modelled as an interface separating products from reactants [30–32], in which all of the effects of the combustion chemistry and related transport effects are confined. Thus, it becomes possible to approximate the thermochemistry via a single Presumed Probability Density Function (PPDF) of a reaction progress variable c (which increases from 0 in the unburned gas to 1 in the fully burned products) and leads to simple closures for a number of

turbulence related terms in the case of premixed turbulent combustion [33]. The most widely used PPDF approach for turbulent premixed flames was proposed by Bray and co-workers [34] and is commonly known as the **Bray Moss Libby (BML) formulation**. This approach makes use of a presumed bi-modal distribution of c with impulses at the unburned and burned mixtures, respectively, and provides elegant closures for several turbulence quantities including statistical moments for velocity and scalar fluctuations within the flame. Bray et al. [35] and Bray and Libby [36] have also provided **simple closures for the mean reaction rate** which are widely used along with the **BML formulation**.

The BML framework has enjoyed some success in predicting turbulent premixed flames in shear flows [37–40], bluff body stabilised flames [41–43], stagnating flows [44] and IC engines [45] but the BML framework has not been widely used for the prediction of FWI within turbulent boundary layers. Hence, **the main aim of this work is to assess the suitability of the BML formulation and the associated reaction rate closures for premixed flames under unity Lewis number conditions interacting with isothermal inert walls within turbulent boundary layers**. It can be expected that the modelling based on the strict flamelet assumption (i.e. high Damköhler number limit) may not be valid in the vicinity of the wall. However, it is worth noting that it is common practice in combustion and turbulence modelling to use closures outside the limits for which they were originally developed, one example is the wide use of gradient diffusion models for closing the turbulent scalar flux. Hence, it is important to determine the extent of agreement or disagreement of the BML model predictions in the near-wall region, and also to assess the range of applicability of the models. This is achieved by interrogating DNS datasets of the FWI process for two different premixed flame configurations, namely: oblique V-flame-wall interaction and head-on quenching within fully developed turbulent boundary layers. The main motivation behind testing the models developed on the BML assumption for FWI in fully developed turbulent boundary layers is three-fold:

1. The near-wall behaviours of the flamelet based closures in the context of RANS are neither widely known nor fully understood for turbulent premixed flames which belong to the corrugated flamelets regime away from the wall. This information is fundamentally important for the purpose of modifying the existing flamelet based models in the near-wall region even when the combustion away from the wall belongs to the corrugated flamelets regime, as in the cases considered in the present work.
2. A priori testing of the existing models is important from the point of view of establishing the limiting behaviour for the models, as some models for FWI under the BML framework were either developed for fully developed turbulent boundary layers at different Re_τ conditions [2,12] or for a different flow condition [10].
3. An estimate for error associated with the model expressions even when accurate turbulence conditions are provided from the DNS data is needed, as some of the models evaluated in the current work have been used in the literature for IC engine simulations where FWI occurs [45].

The rest of the paper is organised as follows: in the next section we briefly describe the mathematical background for the BML formulation and the associated reaction rate closure. This is followed by the description and details of the DNS data, which is then followed by a discussion of the results obtained from the analysis. Finally, the conclusions are drawn and the main results are summarised in the last section.

2. Mathematical background

The **reactive field** is usually expressed in terms of the reaction progress variable as:

$$c \equiv \frac{(Y_{F_R} - Y_F)}{(Y_{F_R} - Y_{F_p})}, \quad (1)$$

where Y_F is the fuel mass fraction and the subscripts R and P indicate the respective values of the fuel in the unburned and fully burned gases. In the case of Reynolds Averaged Navier-Stokes (RANS) or Large Eddy Simulations (LES) of industrial configurations, the Favre averaged or filtered transport equation for c is usually solved. In this work, we focus on the Favre averaged counterpart of the transport equation, which can be expressed as :

$$\frac{\partial \bar{\rho} \tilde{c}}{\partial t} + \frac{\partial \bar{\rho} \tilde{u}_j \tilde{c}}{\partial x_j} = \frac{\partial}{\partial x_j} \left(\rho \alpha_c \frac{\partial c}{\partial x_j} - \bar{\rho} \tilde{u}_j'' \tilde{c}'' \right) + \bar{\omega}_c, \quad (2)$$

where u_j is the j th component of velocity, $\bar{\rho} \tilde{u}_j'' \tilde{c}''$ is the j th component of turbulent scalar flux, $\bar{\omega}_c$ is the mean reaction rate and α_c is the diffusivity of the reaction progress variable respectively. In Eq. (2), $\tilde{Q} = \rho Q / \bar{\rho}$ and $Q'' = Q - \bar{Q}$ represent Favre average and Favre fluctuations of a general quantity Q , respectively, where the overbars indicate Reynolds averaging. The **BML formulation requires a PDF for c to be specified**. The PDF is based on physical arguments and the flame is considered to be made up of thin flamelets; if a probe is inserted into the flame brush at a fixed point then it would pick up reactants for some time and products for the rest of the time [46]. Since the flamelet is very thin, the reacting gas is going to cross the probe only for a very short time interval [46]. The PDF can thus be approximated as [31]:

$$P(c; \mathbf{x}) = \alpha(\mathbf{x}) \delta(c) + \beta(\mathbf{x}) \delta(1 - c) + \gamma(\mathbf{x}) f(c; \mathbf{x}) [H(c) - H(c - 1)], \quad (3)$$

where $\delta(c)$ is the Dirac delta function, $H(c)$ is the Heaviside function, $\alpha(\mathbf{x})$ is the probability of finding reactants, $\beta(\mathbf{x})$ is the probability of finding products and $\gamma(\mathbf{x})$ is the probability of finding reacting gas [31]. Note that α , β and γ are non-negative functions of position \mathbf{x} . The function $f(c; \mathbf{x})$ is a continuous function of the progress variable c and satisfies the condition $\int_0^1 f(c; \mathbf{x}) dc = 1$ [31]. The presumed PDF in Eq. (3) is normalised by integration over c such that [31]:

$$\begin{aligned} \int_0^1 P(c; \mathbf{x}) dc &= \int_0^1 \alpha(\mathbf{x}) \delta(c) dc + \int_0^1 \beta(\mathbf{x}) \delta(1 - c) dc \\ &+ \int_0^1 \gamma(\mathbf{x}) f(c; \mathbf{x}) dc = 1, \end{aligned} \quad (4)$$

thus leading to $\alpha + \beta + \mathcal{O}(\gamma) = 1$ under the limit of large Damköhler number (i.e. $Da \gg 1$) where $\mathcal{O}(\gamma) \sim \mathcal{O}(1/Da)$. Consequently, for large Da the contributions of $\mathcal{O}(\gamma)$ become negligible. The coefficients α and β can then be expressed as [31,34]:

$$\alpha = \frac{1 - \tilde{c}}{1 + \tau \tilde{c}} \text{ and } \beta = \frac{(1 + \tau) \tilde{c}}{(1 + \tau \tilde{c})}, \quad (5)$$

where $\tau = (T_{ad} - T_R)/T_R$ is the heat release parameter with T_R and T_{ad} being the unburned gas temperature and the adiabatic flame temperature, respectively. The expressions for the coefficients α and β can be used to relate the Reynolds averaged progress variable to the Favre averaged progress as [34]:

$$\bar{c} = \frac{(1 + \tau) \tilde{c}}{(1 + \tau \tilde{c})} + \mathcal{O}(1/Da). \quad (6)$$

The BML formulation allows for the evaluation of variance of the progress variable c''^2 as:

$$\tilde{c}''^2 = \tilde{c}(1 - \tilde{c}) + \mathcal{O}(1/Da). \quad (7)$$

The PPDF framework of the BML formulation does not enable the evaluation of the mean reaction rate $\bar{\omega}_c$ as the main assumption of the BML formulation is that the flame-interior contribution to the PDF of c vanishes as $\gamma \rightarrow 0$. Bray et al. [35] and Bray and Libby [36] have provided a solution to this problem by developing a theoretical framework based on the flamelet crossing frequency approach and expressed the mean reaction rate in terms of the Flame Surface Density (FSD) - which is taken to be the generalised FSD $\Sigma_{gen} = |\nabla c|$ in this work, based on the definition of Boger et al. [47] - and the mean consumption rate per unit flame surface area Ω_c . Thus, the resulting mean reaction rate can be expressed as [48–51]:

$$\bar{\omega}_c = \Omega_c \Sigma_{gen}, \quad (8)$$

where the quantity Ω_c is defined as:

$$\Omega_c = I_0 \rho_R S_L. \quad (9)$$

In Eq. (9), ρ_R is the unburned gas density, S_L is the unstretched laminar burning velocity and I_0 is the stretch factor [52]. The generalised FSD can be expressed in terms of the flame orientation factor σ_y , which is related to the angle between the normal vectors of \bar{c} isosurface and the flame surface, and the flame crossing per unit length n_y as:

$$\Sigma_{gen} = \frac{n_y}{\sigma_y}. \quad (10)$$

This leads to the following expression for the FSD [45,53,54]:

$$\Sigma_{gen} = \frac{g \bar{c} (1 - \bar{c})}{\sigma_y L_y}, \quad (11)$$

where g is a model parameter of the order of unity, L_y is the integral length scale of the flamelet crossing process, also known as the flamelet length scale. Using the expression for \bar{c} from Eq. (6) in Eq. (11) leads to:

$$\Sigma_{gen} = \frac{g \tilde{c} (1 - \tilde{c})}{\sigma_y L_y} \frac{(1 + \tau)}{(1 + \tau \tilde{c})^2}. \quad (12)$$

3. Direct Numerical Simulation Data

In this work, DNS of two different flame configurations have been considered under **unity Lewis number and low Mach number** conditions. The first configuration consists of the **oblique flame-wall interaction of a V-flame with inert isothermal walls** in a **turbulent channel flow**, while the second configuration consists of a **statistically planar flame propagating into a fully turbulent boundary layer and interacting with an inert isothermal wall**. A well-known three-dimensional compressible DNS code SENGA+ [55] has been used to simulate premixed flame-wall interaction with inert isothermal walls in fully developed turbulent boundary layers. The code employs high-order finite-difference (10th order for internal points and gradually decreasing to 2nd order at the non-periodic boundaries) and Runge–Kutta (3rd order explicit) schemes for spatial differentiation and time advancement, respectively. The governing equations of mass, momentum, energy, and species mass fractions are solved in a non-dimensional form and a single-step irreversible reaction (1 unit mass of *Fuel* + s unit mass of *Oxidiser* \rightarrow $(1 + s)$ unit mass of *Products*) (where s is the stoichiometric oxidiser-fuel ratio) is used for the purpose of computational economy. This treatment for chemical reaction has been employed in several previous studies involving head-on quenching simulations of premixed turbulent flames under isotropic turbulence [3–10], head-on quenching in a turbulent channel flow without density change across the flame [11,12] and a V-flame configuration [1,2]. It should be noted here that the issues related to heat release in the near wall region and its implications on the use of single-step chemistry have been discussed in

detail by Lai et al. [8] from the point of view of wall heat flux and wall Peclet number, which are consistent with the experimental findings [56–58] when using single-step chemistry, and by Ahmed et al. [4] from the point of view of the underlying fluid-dynamical effects during FWI. As far as the heat release in the near wall region is concerned, it has been shown by Gruber et al. [13] that the underlying fluid dynamics and the global flame behaviour for the V-flame is similar to the earlier findings of Alshaalan and Rutland [1,2] who employed single-step chemistry, similar to the one used in the current work. It has been shown by Lai et al. [8] that in the case of the stoichiometric methane-air flames - which is the representative mixture used in the current simulations - during head-on quenching under decaying isotropic turbulence, the flame dynamics is not affected by the choice of the chemical mechanism and in the case of detailed chemistry simulation an increase in CO and HO₂ production is seen which is consistent with the recent DNS of a premixed V-flame in a turbulent channel flow employing a detailed chemical mechanism for methane by Jiang et al. [59]. This implies that the turbulent boundary layer flow does not have a significant influence on the behaviour of chemistry during the FWI process of premixed flames when compared with the premixed head-on quenching flames under decaying isotropic turbulence and the flame dynamics from single-step chemical mechanism is similar to the flame dynamics from the detailed chemical mechanism. In the recent experimental results of Jainski et al. [24], it has been shown that the models developed by using single-step chemistry DNS are able to represent global features of the near-wall FSD profiles obtained in experiments. It is also worth noting that the BML formulation does not require information for detailed chemistry and thus the use of single step chemistry does not limit the scope of the current analysis. Moreover, the choice of simple chemistry removes the uncertainty associated with the definition of reaction progress variable in the context of a detailed chemical mechanism.

The current simulations are representative of a stoichiometric methane-air mixture under atmospheric conditions, hence standard values of the Zeldovich number $\beta_z = T_a(T_{ad} - T_R)/T_{ad}^2$ (where T_a is the activation temperature), Prandtl number Pr , and ratio of specific heats γ_s (i.e., $\beta_z = 6.0$, $Pr = 0.7$, and $\gamma_s = 1.4$) are used where the Lewis numbers of all the species are taken to be unity. It has recently been shown in a DNS study of statistically planar methane-air flames with detailed chemistry and transport [60] that the global Lewis number remains close to unity and the leading-order response of the flame speed to turbulence is primarily driven by the global Lewis number even under very intense turbulence conditions which justifies the use of unity Lewis number in this work. The heat release parameter τ is taken to be 2.3 for the flames considered here, which corresponds to preheating of reactants to a temperature of $T_R = 730$ K. This value of T_R and the resulting τ is consistent with the earlier detailed chemistry DNS of FWI in the case of a premixed V-flame in a turbulent channel flow [13], turbulent boundary layer flashback [15,17–19] and single-step chemistry premixed V-flame DNS with FWI [1,2] and without FWI [61]. In order to perform wall bounded flow simulations, the isothermal no-slip wall boundary condition is implemented in SENGA+ according to the Navier Stokes Characteristic Boundary Conditions (NSCBC) technique [62]. In this case all the velocity components vanish at the wall and the temperature value is imposed at the wall. No relation is imposed for heat fluxes or the viscous stresses and the species mass fluxes are set to zero in the wall normal direction. In this case, the local one dimension inviscid (LODI) relations simplify to $\mathcal{L}_1 = \mathcal{L}_5$ and $\mathcal{L}_1 = \mathcal{L}_2 = \mathcal{L}_3 = \mathcal{L}_4 = \mathcal{L}_{5+k} = 0$, where \mathcal{L}_i is the amplitude variation of the i th characteristic wave crossing the boundary, \mathcal{L}_1 and \mathcal{L}_2 are associated with acoustic waves in the wall normal direction, where \mathcal{L}_2 is associated with the advection of entropy, while \mathcal{L}_3 and \mathcal{L}_4 are

associated with advections in wall tangential directions and \mathcal{L}_{5+k} is associated with the advection of the k th species. The density at the wall is obtained from the solution of the continuity and the species transport equations. The derivatives of the species needed to solve the system of equations at the wall are obtained by using a 2nd order one-sided scheme.

3.1. Non-reacting turbulent channel flow

The initial turbulence conditions for both simulations and the inflow conditions for the V-flame simulation are obtained by performing an auxiliary DNS of inert fully developed turbulent-plane channel flow driven by a stream-wise constant pressure gradient. An overall momentum balance can be used to show that the pressure gradient is directly related to the shear stress as $-\partial p/\partial x = \rho u_\tau^2/h$, where $u_\tau = \sqrt{|\tau_w|/\rho}$ is the friction velocity, $\tau_w = \mu \partial u / \partial y|_{y=0}$ is the wall shear stress, h is the channel half height, p is the pressure and μ is the dynamic viscosity of the fluid. The bulk Reynolds number $Re_b = \rho u_b h / \mu$ for this simulation is 3285, where $u_b = 1/2h \int_0^{2h} u dy$, and the wall friction based Reynolds number $Re_\tau = \rho u_\tau h / \mu$ is 110. The current grid spacing ensures that the minimum non-dimensional distance to the wall $y^+ = \rho u_\tau y / \mu$, where y is the distance from the wall, is at most $y^+ = 0.6$ and the region $y^+ < 1$ has approximately two grid points which ensures appropriate resolution of the boundary layer as recommended by Moser et al. [63]. The domain size for this channel is $10.69h \times 2h \times 4h$ and $1920 \times 360 \times 720$ equidistant grid points are used to discretise the computational domain.

3.2. V-flame in a turbulent channel flow

The V-flame simulation is performed by placing a flame holder in the fully developed turbulent channel flow at $y^+ = 55$ from the bottom wall (i.e. $y = 0.5h$) with an approximate radius of $R_{fth} \approx 0.2\delta_{th}$ ($\delta_{th} = (T_{ad} - T_R)/\max|\nabla T|_L$, where the subscript L represents the laminar flame quantities) and the centre positioned at $x/h = 0.83$ from the inlet of the channel. This location for the flame holder ensures that the flame interacts with the bottom wall at a reasonable distance and also that the viscous boundary layer is not influenced by the flame holder and any effects seen in the boundary layer downstream of the flame holder are due to thermal expansion arising from chemical reaction. At the flame holder, the species, temperature and velocity distributions are imposed using a presumed Gaussian function following Dunstan et al. [61]. Further details on the implementation of the flame holder for this simulation are available in [14]. The velocity fluctuations introduced at the inflow of the reacting channel are obtained by temporal sampling of the temporally evolving turbulence at a fixed streamwise location of auxiliary non-reacting channel flow simulation. Note that the time step chosen for the non-reacting simulation, while the data is being sampled, is the same as that of the reacting flow simulation. This approach, which permits eddies to develop on the boundary, provides a more realistic description of turbulence for developed boundary layer flows when compared with the technique relying on Taylor's hypothesis.

The simulation set-up for the V-flame is shown in Fig. 1. In the x and y directions modified Navier-Stokes characteristic boundary conditions (NSCBC) due to Yoo and Im [64] are used. The boundary conditions are inflow with specified density and velocity components at $x = 0$ and partially non-reflecting outflow at $x = 10.69h$ planes; no slip conditions are imposed for velocity at the walls (i.e. $y = 0$ and $y = 2h$), while the temperature boundary condition is specified using Dirichlet (i.e. $T_w = T_R$, T_w is the wall temperature) conditions. The boundaries in z direction are treated as periodic. The walls are assumed to be inert and impermeable, hence normal mass flux for all species is set to zero at the walls. The laminar

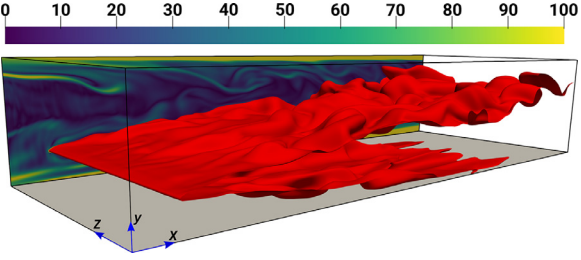


Fig. 1. V-flame (case-A) with isothermal wall boundary conditions. The isosurface coloured in red represents $c = 0.5$. The instantaneous normalised vorticity magnitude Ω is shown on the $x - y$ plane at $z/h = 4$. The grey surface denotes the bottom wall. (For interpretation of the references to colour in this figure legend, the reader is referred to the web version of this article.)

flame speed to friction velocity ratio $S_L/u_\tau = 0.7$ and the laminar flame thermal thickness δ_{th} is resolved using approximately 8 grid points. The simulations have been performed for approximately 3 flow-through times and the data has been sampled after 1 flow through time once the initial transience have decayed. Note that under the current flow conditions 1 flow-through time is enough to obtain a statistically stationary solution for the mean turbulent kinetic energy statistics. The instantaneous flame structures represented by the $c = 0.5$ isosurface along with the normalised vorticity magnitude $\Omega = \sqrt{\omega_i \omega_i} \times h/u_\tau$ (where ω_i is the component of vorticity) are shown in Fig. 1. The influence of the walls on Ω and the existence of wall ejections due to introduction of the fully developed boundary layer at the inflow are clearly visible. This simulation is referred to as Case-A later on in the paper.

In this case the Reynolds averaged quantities, Favre averaged quantities, correlations involving Reynolds fluctuations (denoted by $Q' = Q - \bar{Q}$) and Favre fluctuations have been evaluated by time averaging and subsequently using spatial averaging in the periodic (z) direction at a given x location, where Q refers to a general quantity. The results are reported in terms of y/h values as y^+ in the case of the reacting channel varies with axial distance due to velocity acceleration caused by thermal expansion effects. The data has been analysed at $y/h = 0.005$, $y/h = 0.044$, $y/h = 0.088$ and $y/h = 0.18$ locations corresponding to $y^+ \approx 0.6$, $y^+ \approx 5$, $y^+ \approx 10$ and $y^+ \approx 20$ respectively. These y^+ values have been evaluated based on the friction velocity for the corresponding non-reacting channel flow configuration.

3.3. Planar flame in a turbulent boundary layer

This simulation is representative of a head-on quenching process of a premixed flame in a fully developed turbulent boundary layer and is similar to the earlier work of Bruneaux et al. [11,12] in a constant density turbulent channel flow. It is perhaps better to avoid a periodic channel flow configuration in the context of variable density reacting flow simulations because it leads to increased pressure within the domain in the absence of a non-reflecting outflow boundary. Thus, the current configuration employs a partially non-reflecting outflow boundary to avoid thermodynamic pressure rise during the course of the simulation. Another aim here is to be able to keep the turbulence characteristics (i.e. Re_τ) of the boundary layer as close to the V-flame case as possible which may not be achievable under a zero pressure gradient spatially developing boundary layer. To achieve these aims, the solution from the fully developed turbulent channel flow up to $y/h = 1.33$ in all of the x and z directions has been used to initialise the simulation. The domain size for this configuration is taken to be $10.69h \times 1.33h \times 4h$, which is discretised on $1920 \times 240 \times 720$ equidistant grid points. The boundary conditions for this case are imposed as periodic in the x and z directions and a mean streamwise pressure gradient

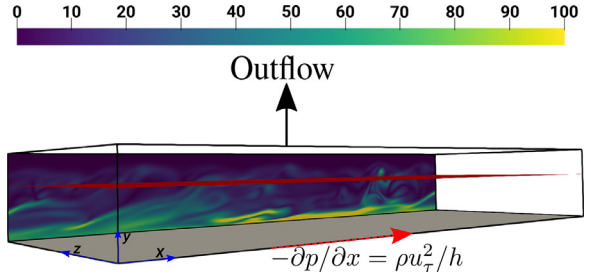


Fig. 2. Schematic of the computational domain and the initial conditions used for the head-on quenching planar flame in a turbulent boundary layer (Case-B). The isosurface coloured in red represents initial conditions for $c = 0.5$. The instantaneous normalised vorticity magnitude Ω is shown on the $x - y$ plane at $z/h = 4$. The grey surface denotes the wall. (For interpretation of the references to colour in this figure legend, the reader is referred to the web version of this article.)

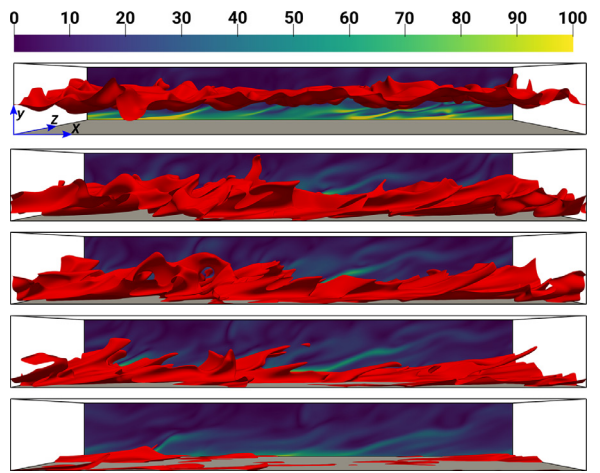


Fig. 3. Head-on quenching with isothermal wall boundary conditions at different time instants. From top to bottom $t/t_f = 4.20$, $t/t_f = 10.50$, $t/t_f = 11.55$, $t/t_f = 12.60$, $t/t_f = 14.70$. The isosurface coloured in red represents $c = 0.5$. The instantaneous normalised vorticity magnitude Ω is shown on the $x - y$ plane at $z/h = 4$. (For interpretation of the references to colour in this figure legend, the reader is referred to the web version of this article.)

is applied in the x direction to maintain the shear rate at the wall which is representative of $Re_\tau = 110$ conditions for the duration of the reacting flow simulation. The pressure gradient has the same expression as for the non-reacting turbulent channel flow in Section 3.1. The boundaries in the y direction are treated as wall at $y = 0$ where a no slip condition is imposed for velocity, while the temperature boundary condition is specified using Dirichlet (i.e. $T_w = T_R$) condition. An outflow boundary condition is specified at $y = 1.33h$ using the NSCBC conditions as defined by Yoo and Im [64]. This procedure is necessary as the influence of the flame configuration can only be investigated if the turbulence characteristics are maintained as close as possible across the different configurations. This has been confirmed by comparing the non-dimensional velocity profiles for a non-reacting turbulent boundary layer under the aforementioned conditions with the turbulent channel flow results and no significant differences were observed during the time needed for the flame to quench in the corresponding reacting flow simulation. A schematic of the flow configuration along with the initial conditions for turbulence and the flame is provided in Fig. 2, where the initial normalised vorticity magnitude Ω is high in the near wall region signifying the initial conditions of the boundary layer.

An initially fully developed laminar flame from a prior 1-D flame simulation is interpolated onto the 3-D grid and specified in a manner that $c = 0.5$ is centred at $y/h \approx 0.85$. Note that the

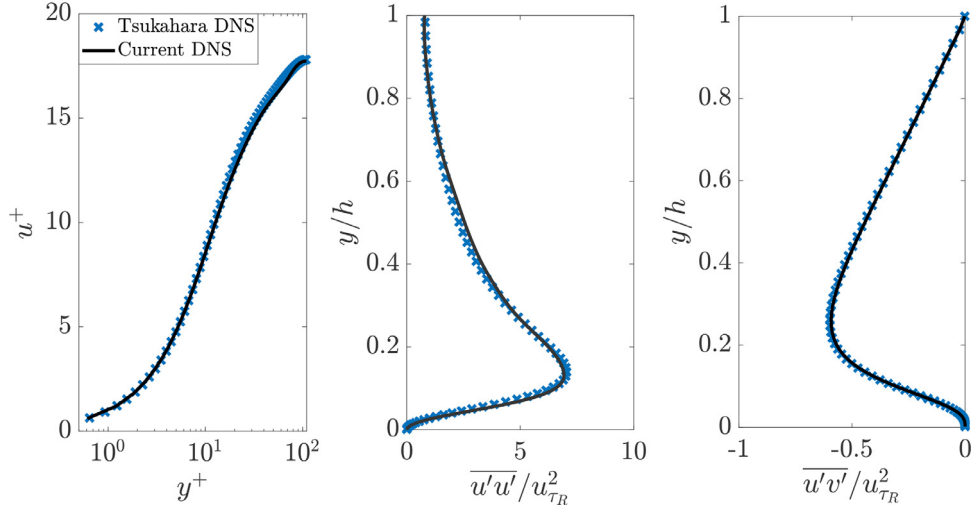


Fig. 4. Mean velocity and Reynolds stresses in the auxiliary channel flow simulation compared with the DNS of Tsukahara et al. [65].

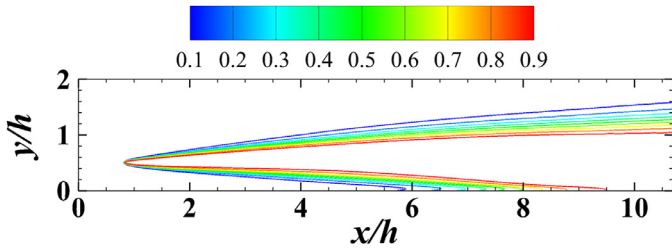


Fig. 5. Contours of the Favre mean progress variable \tilde{c} for case-A.

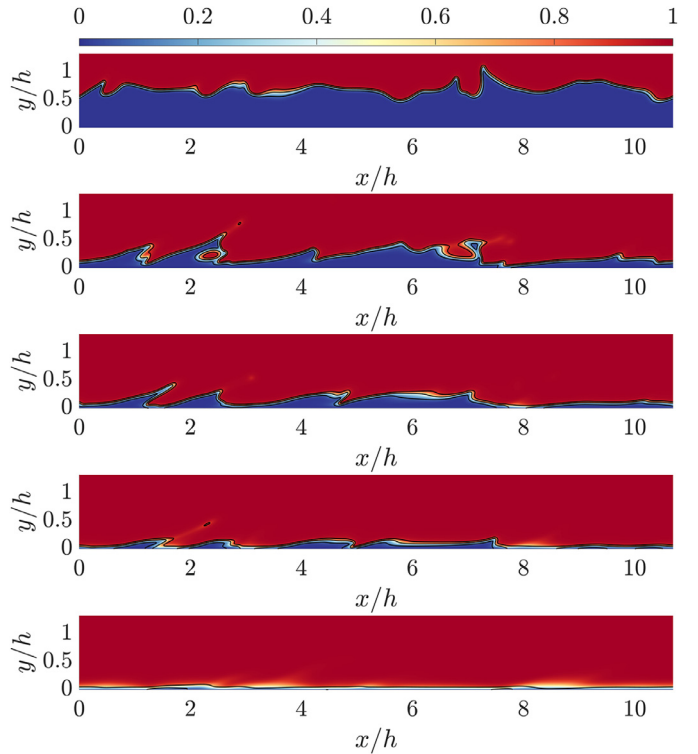


Fig. 6. Variations of the instantaneous progress variable $c = 0.1, 0.5, 0.9$ (from bottom to top) superimposed on the instantaneous distribution of non-dimensional temperature T on the mid-plane in the spanwise z direction for different time instants (from top to bottom $t/t_f = 4.20$, $t/t_f = 10.50$, $t/t_f = 11.55$, $t/t_f = 12.60$, $t/t_f = 14.70$) for case-B.

initial flame is specified such that the reactant side of the flame is facing the wall, while the product side of the flame is facing the outflow boundary in the y direction. It should be recognised here that the choice of the initial flame location and the length of the domain in the y direction is made based on the fact that the flame must remain sufficiently away from the outflow boundary at all times, while giving the flame enough time to wrinkle before interacting with the wall to obtain meaningful FWI statistics for a turbulent premixed flame. Similar to the V-flame (case-A) defined in Section 3.2 the ratio $S_L/u_\tau = 0.7$ and δ_{th} is resolved using approximately 8 grid points. In this case the boundary layer evolves slightly as the simulation progresses, but the overall simulation time remains of the order of 2.0 flow-through times based on the maximum axial mean velocity, which is equivalent to 21.3 flame time scales defined as $t_f = \delta_{th}/S_L$. During this time the flame propagates into the reactants and moves towards the isothermal wall, consequently interacting with the isothermal wall and quenching due to heat loss at the wall.

During the post processing of this simulation the Reynolds averaged quantities, Favre averaged quantities, correlations involving Reynolds fluctuations and Favre fluctuations have been evaluated by spatial averaging in the periodic (x and z) directions for each snapshot. The results are reported in terms of the normalised simulation time t/t_f , which is representative of the mean flame location in the y direction at a given snapshot. Figure 3 shows the time evolution of the flame-boundary layer interaction at different time instants in the simulation. The instantaneous flame structures represented by the $c = 0.5$ isosurface along with the normalised vorticity magnitude Ω . The vorticity generated in the vicinity of the wall within the turbulent boundary layer can be seen in Fig. 3. This simulation is referred to as case-B in the subsequent sections of the paper.

4. Results and discussion

4.1. Flow behaviour

The non-reacting auxiliary channel flow simulation has been compared with the results of Tsukahara et al. [65]¹ at $Re_\tau = 110$ and an excellent agreement has been obtained as shown in Fig. 4, where $u^+ = \bar{u}/u_{\tau_R}$ and u_{τ_R} is the mean wall friction velocity in the non-reacting simulation. In the case of reacting flow simulations, it is useful to quantify the flame quenching distance δ_Q to

¹ Database available online at: <https://www.rs.tus.ac.jp/t2lab/db/>

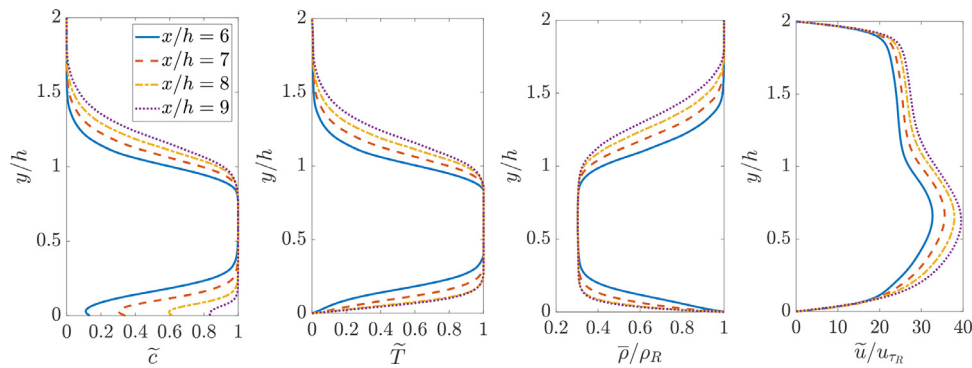


Fig. 7. Variations of the Favre mean progress variable, Favre mean non-dimensional temperature, normalised mean density and normalised Favre mean streamwise velocity at different x/h locations in case-A.

establish the accuracy of the simulations in the two flame configurations. In this case, a quenching Peclet number $Pe_Q = \delta_Q/\delta_z$ is used ($\delta_z = \alpha_{T_R}/S_L$ is the Zeldovich flame thickness, where α_{T_R} is the unburned gas thermal diffusivity). Here δ_Q is taken to be the minimum wall-normal distance of the non-dimensional temperature $T = 0.75$ isosurface (i.e. the value of the temperature isosurface at which the maximum heat release rate is obtained for an unstrained laminar premixed flame for the present thermochemistry), where $T = (\hat{T} - T_R)/(T_{ad} - T_R)$ is the non-dimensional temperature and \hat{T} is the local dimensional temperature at a given point. The minimum Peclet number Pe_Q , which represents the minimum wall normal distance of the flame signifying the flame quenching distance, in case-A is found to be 1.82, while in case-B it is equal to 1.71 which is close to the conventional 1-D laminar head-on quenching value of 2.19 and is consistent with the earlier studies [6,66]. These values can be expressed in terms of y/h values and are 0.034, 0.032 and 0.04 for case-A, case-B and the conventional 1-D laminar head-on quenching flame respectively.

Figure 5 shows the Favre averaged progress variable distributions for case-A. It can be seen that the flame interacts with the bottom wall far downstream of the flame holder and the flame is stretched along the wall in the regions of interaction with the wall (i.e. $5.5 < x/h < 10$). This behaviour of the flame is expected due to the diffusion of the reactants along the wall and is consistent with the earlier findings of Alshaalan and Rutland [1,2] based on DNS with simple chemistry representing hydrocarbon-air mixtures and detailed chemistry hydrogen-air DNS by Gruber et al. [13], who demonstrated that the V-flame thickens in the near wall region which may result in departures from the strict flamelet limit. The departure from the strict flamelet behaviour in the case of head-on quenching has been demonstrated by Lai and Chakraborty [6] and Zhao et al. [20] using simple chemistry DNS, which was also confirmed by Lai et al. [8] using detailed chemistry methane-air head-on quenching DNS data.

Figure 6 shows the instantaneous non-dimensional temperature field, superimposed with contour lines of c for case-B on the $x-y$ mid-plane at $t/t_f = 4.20, 10.50, 11.55, 12.60$ and 14.70 . It can be seen from Fig. 6, that the flame gets wrinkled by the turbulent flow features within the boundary layer as it propagates towards the wall. It can also be seen that the thermal boundary layer starts to develop as the flame starts to interact with the isothermal wall.

The behaviours of the mean values of density, Favre mean values of streamwise velocity, progress variable and non-dimensional temperature are shown in Fig. 7 for case-A at different x/h locations downstream of the flame holder. A decoupling between the progress variable and temperature can be seen at the bottom wall due to quenching as a result of the heat loss at the isothermal wall. The mean velocity increases with the downstream distance from the flame holder due to thermal expansion effects, as shown

in Fig. 7. Figure 8 shows the mean values of density, and Favre mean values of streamwise velocity, progress variable and non-dimensional temperature for case-B at different time instants during the simulation. It can be seen from Fig. 8 that the mean flame brush, represented by \tilde{c} , becomes thicker due to interaction with the turbulence within the boundary layer and also propagates towards the wall as time progresses eventually interacting with the wall and quenching due to heat loss at the wall. The main difference between the mean profiles for the two configurations exists in the mean axial component of velocity \tilde{u} . In case-B, \tilde{u} is not significantly affected because the thermal expansion due to the flame is in the wall normal direction as opposed to being parallel to the wall as in case-A. In both flow configurations, when the flame is away from the wall, the values for Damköhler number remain high (i.e. $Da >> 1$) and Karlovitz number remains small (i.e. $Ka \ll 1$). It should also be recognised here that the integral length scale based on two-point correlations becomes large as the wall is approached for low Re_τ boundary layers [67]. This indicates that when the length scale based on two-point correlations is used the Damköhler number assumes infinitely large values, whereas vanishingly small values of Karlovitz number are obtained in the vicinity of the wall. Thus, the flames in case-A and case-B nominally belong to the corrugated flamelets regime away from the wall.

It is important to note that boundary conditions for species mass fraction and temperature are different at the isothermal wall. The species mass fraction follows a Neumann boundary condition, whereas a Dirichlet boundary condition is specified for temperature. As a result of flame quenching, the unburned reactants diffuse from the near-wall region and their mass fraction drops at the wall, which leads to an increase in the value of the progress variable. This behaviour has been reported in several previous analyses on flame-wall interaction involving both simple [5–7,10] and detailed [8] chemical mechanisms. Moreover, this behaviour was also reported in previous DNS investigations on V-flame-wall interaction in the case of single-step chemistry by Alshaalan and Rutland [1,2] and detailed chemistry by Gruber et al. [13]. This trend is also shown in the recent experimental results of Jainski et al. [25,26]. As there are several mean flow features of the flame, which are not similar to the conventional unconfined flames without FWI, it is important to investigate these flames further for the applicability of the BML framework.

4.2. Probability density function of the progress variable

The PDF distributions for c at different values of \bar{c} and \tilde{c} sampled at different y/h locations away from the bottom wall in case-A are presented in Fig. 9. It can be seen from Fig. 9 that in case-A the PDF distributions corresponding to \bar{c} and \tilde{c} are similar for a given y/h location. It can also be noticed from Fig. 9 that as

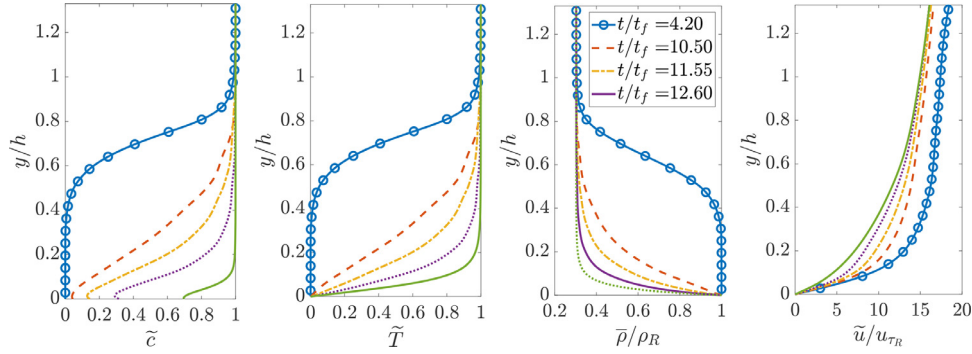


Fig. 8. Variations of the Favre mean progress variable, Favre mean non-dimensional temperature, normalised mean density and normalised Favre mean streamwise velocity at different time instants in case-B.

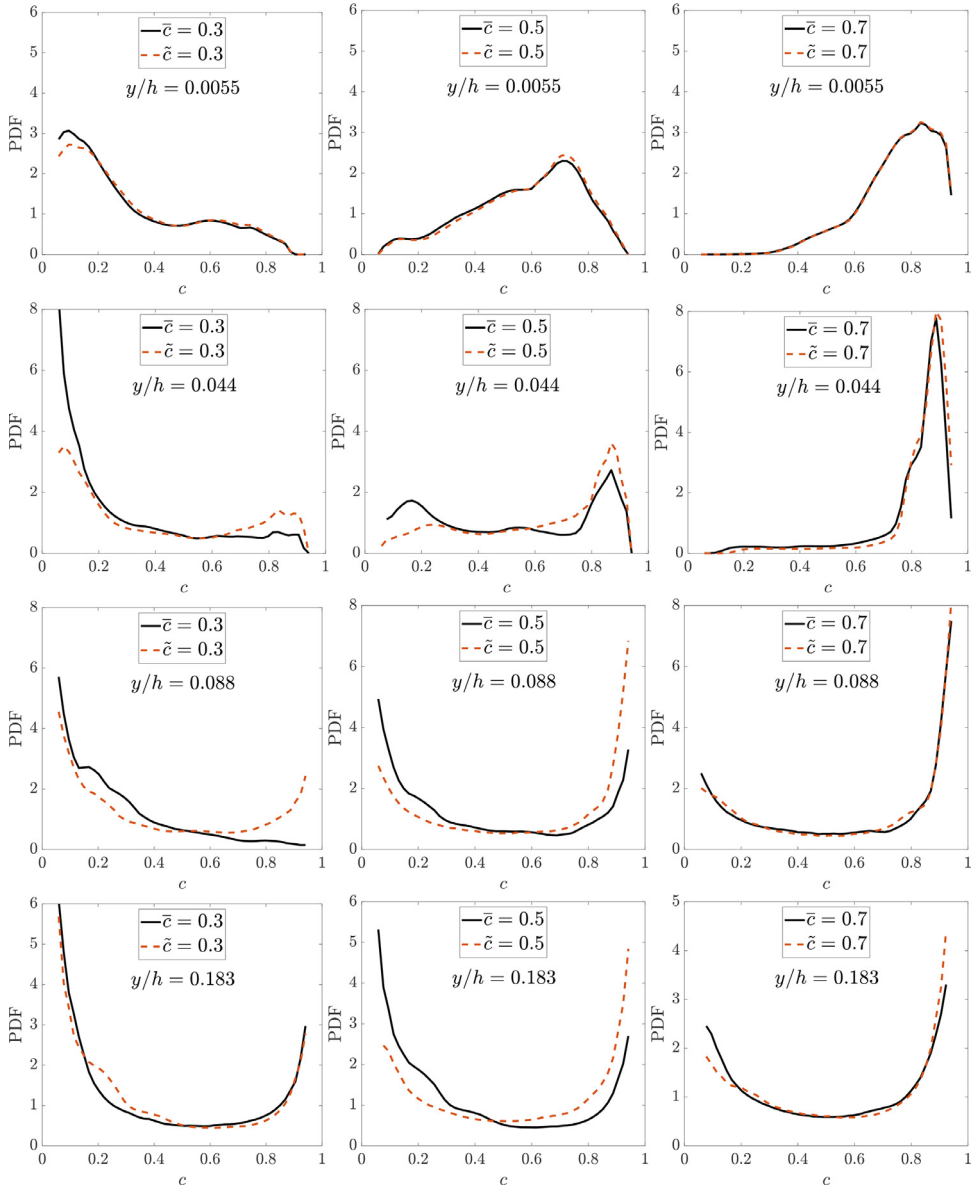


Fig. 9. Probability density function (PDF) distributions for c at $\bar{c} = 0.5, 0.3, 0.7$ and $\tilde{c} = 0.5, 0.3, 0.7$ for different distances away from the wall at $y/h = 0.0055, y/h = 0.044, y/h = 0.088$ and $y/h = 0.183$ in case-A.

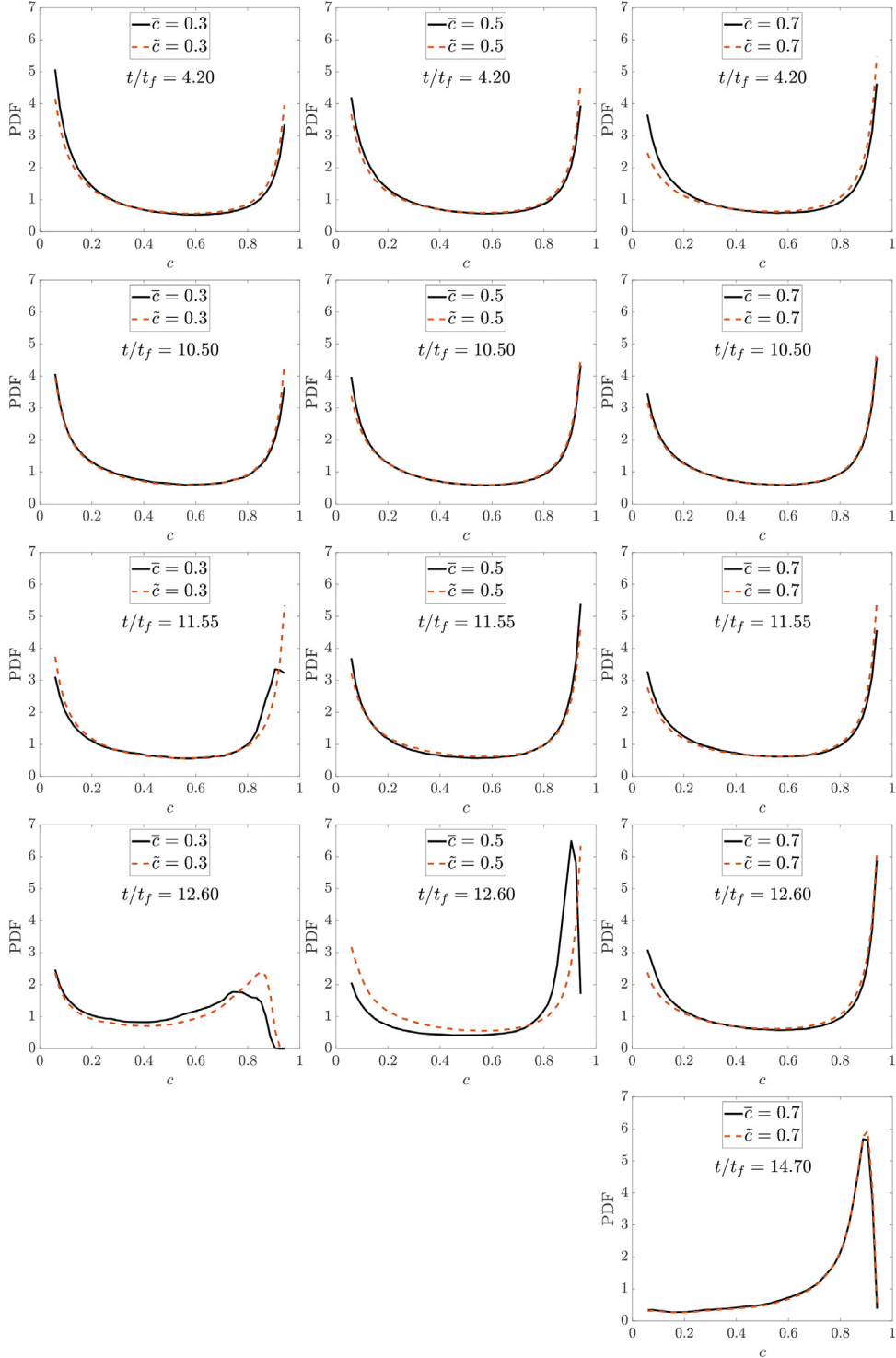


Fig. 10. Probability density function (PDF) distributions for c at $\bar{c} = 0.5, 0.3, 0.7$ and $\tilde{c} = 0.5, 0.3, 0.7$ in case-B at different times $t/t_f = 4.20$, $t/t_f = 10.50$, $t/t_f = 11.55$, $t/t_f = 12.60$ and $t/t_f = 14.70$ in case-B.

the distance from the wall increases, the PDFs tend to show a bi-modal distribution, whereas in the near wall region the PDFs tend to exhibit a mono-modal behaviour at the leading and trailing edges of the flame and beta type distribution in the interior of the flame. This deviation from the bi-modal behaviour prevails up to $y/h = 0.088$. The PDF distributions for c at different \bar{c} and \tilde{c} values sampled at different t/t_f for case-B are presented in Fig. 10. It can be seen that the PDF behaviour is similar for both \bar{c} and \tilde{c}

sampling at all times. The bi-modal behaviour can be observed at earlier times which implies that the flame is away from the wall. At later times when substantial FWI occurs (i.e. at $t/t_f = 12.60$) the PDF behaviour starts to deviate from the bi-modal nature at the leading edge of the flame, while the rest of the flame still tends to retain the bi-modal distribution. With the progress of time the flame quenches due to the heat loss at the wall and also due to the consumption of the reactants, consequently the PDF distribu-

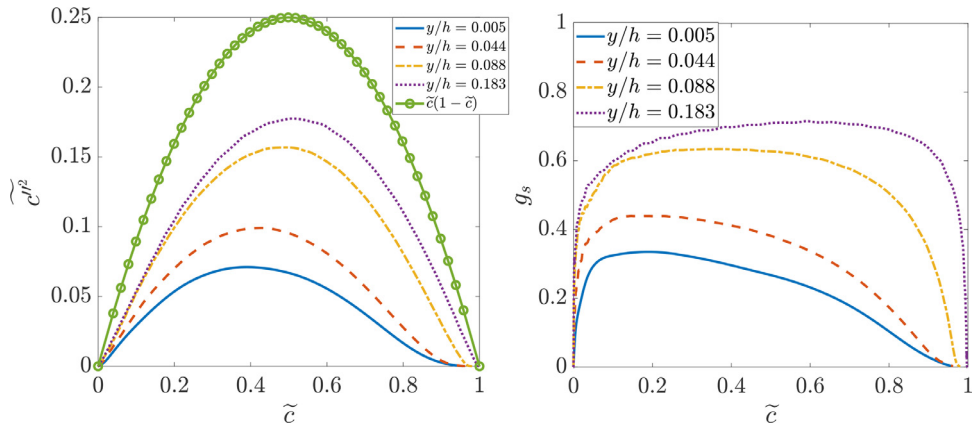


Fig. 11. Behaviour of variance of the progress variable $\tilde{c}^{\prime\prime}$, $\tilde{c}(1 - \tilde{c})$ and the segregation factor for case-A at different distances away from the wall.

tion for c tends to take a mono-modal distribution for high values of \tilde{c} and samples for small values of \tilde{c} become increasingly unavailable. This is in contrast to case-A where a constant supply of reactants sustains the flame and leads to a different behaviour for the PDF of c in the vicinity of the wall.

As evident from Figs. 9 and 10 the PDFs of c differ significantly between the two flow configurations in the near wall region. These differences exist, as in case-A a constant supply of reactants sustains the flame, whereas in case-B the flame consumes the reactants as it approaches the wall and FWI occurs, resulting in flame quenching not only due to the heat loss at the wall but also due to the complete consumption of the reactants within the domain. In both cases there are significant departures from the strict BML limit when the flame is interacting with an isothermal wall. Furthermore, it is also evident that these departures are different for different flame or flow configurations during FWI. In both cases the flame brush tends to thicken as it approaches the wall partly due to the turbulence within the turbulent boundary layer and partly due to the flame interacting with the wall. Note that in both cases the highest mean flame brush thickness is observed at the wall which is due to the diffusion processes occurring on the wall surface.

4.3. Behaviour of the Favre averaged variance of the progress variable

The departures from the strict BML limit can be further quantified by analysing the segregation factor defined as:

$$g_s = \frac{\tilde{c}^{\prime\prime}}{\tilde{c}(1 - \tilde{c})}, \quad (13)$$

which returns a value of unity for the strict bi-modal shape for $P(c; \mathbf{x})$ (i.e. the strict BML limit) and decreases as the departure from the bi-modal distribution occurs. The behaviours of $\tilde{c}^{\prime\prime}$, $\tilde{c}(1 - \tilde{c})$ and g_s are presented in Fig. 11 for case-A at different y/h locations away from the wall. It can be seen from Fig. 11 that the $\tilde{c}(1 - \tilde{c})$ has a maximum value of 0.25, whereas the maximum value of $\tilde{c}^{\prime\prime}$ remains smaller than 0.25. The value for $\tilde{c}^{\prime\prime}$ decreases with decreasing distance from the wall as the flame wrinkling due to turbulence decreases and the flame brush becomes thicker in the vicinity of the wall. The behaviour of the segregation factor is also shown in Fig. 11 for case-A. Away from the wall at $y/h = 0.183$, $g_s \approx 0.7$, whereas it tends to decrease with distance as the wall is approached. This implies that case-A deviates from the strict BML limit in the near wall region.

Figure 12 shows the behaviour of $\tilde{c}^{\prime\prime}$, $\tilde{c}(1 - \tilde{c})$ and g_s for case-B. It can be seen from Fig. 12 that in contrast to case-A, the max-

imum value of $\tilde{c}^{\prime\prime}$ tends to 0.2 during the early stages of the FWI process. Note that no data exists for $\tilde{c}^{\prime\prime}$ at small values of \tilde{c} due to the flame quenching process. The comparison of segregation factor for case-B at different time instants presented in Fig. 12 shows that the value of $g_s \approx 0.8$ when the flame is away from the wall and also during the early stages of FWI. At the later stages of FWI (e.g. $t/t_f = 14.70$) the maximum value of g_s decreases due to flame quenching caused by heat loss. This behaviour of g_s implies that during head-on quenching of a planar flame in a turbulent boundary layer, the flame deviates away from the strict BML limit at later stages of FWI even when the combustion is representative of the corrugated flamelets regime away from the wall. The behaviour of $\tilde{c}^{\prime\prime}$ is significantly different for the two flow configurations as in case-A the value of $\tilde{c}^{\prime\prime}$ and g_s decreases rapidly as the flame approaches the wall, while in case-B $\tilde{c}^{\prime\prime}$ and g_s are not significantly affected at the early stages of FWI and only decrease as the flame is close to quenching. This is due to the fact that the product side of the flame in case-B remains significantly away from the wall at early stages of FWI and interacts with the turbulence in the boundary layer for longer when compared with the V-flame in case-A. Furthermore, the values of $\tilde{c}^{\prime\prime}$ and g_s at small values of \tilde{c} do not exist during FWI in case-B due to flame quenching caused by the cold wall and also due to the consumption and diffusion of the reactants in the near wall region.

4.4. Behaviour of the Reynolds averaged progress variable

The Reynolds averaged progress variable \bar{c} can be obtained via the BML framework through Eq. (6) under the strict BML limit (i.e. bi-modality) and any departures from that limit have implications on the validity of the expression in Eq. (6). It is possible to manipulate Eq. (6) and using the expression in Eq. (7) to obtain an alternative expression as [68,69]:

$$\bar{c} = \tilde{c} + \frac{\tau \tilde{c}^{\prime\prime}}{1 + \tau \tilde{c}}. \quad (14)$$

Another expression for \bar{c} has been proposed by Chakraborty and Cant [70] which also includes the influence of Lewis number (Le). This expression is derived from the expression in Eq. (7) and replacing τ by $\tau g_s^a Le^{-b}$ as [70]:

$$\bar{c} = \frac{(1 + \tau g_s^a Le^{-b}) \tilde{c}}{1 + \tau g_s^a Le^{-b} \tilde{c}}, \quad (15)$$

where $a = 1.5$ and $b = 0.26$ in the case of $Da < 1$ flames. Figure 13 shows the variation of \bar{c} at different y/h locations away from the wall and the predictions from the expressions in Eqs. (6), (14) and

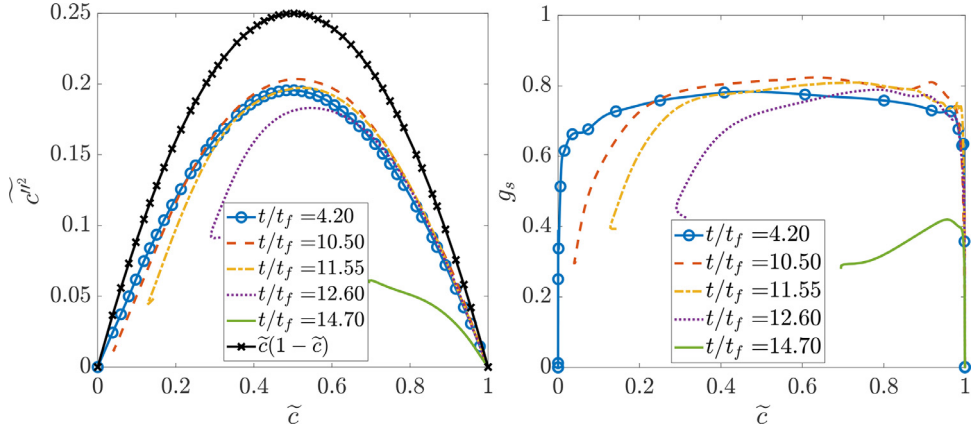


Fig. 12. Behaviour of variance of the progress variable \tilde{c}^2 / \tilde{c} , $\tilde{c}(1 - \tilde{c})$ and the segregation factor for case-B at different time instances.

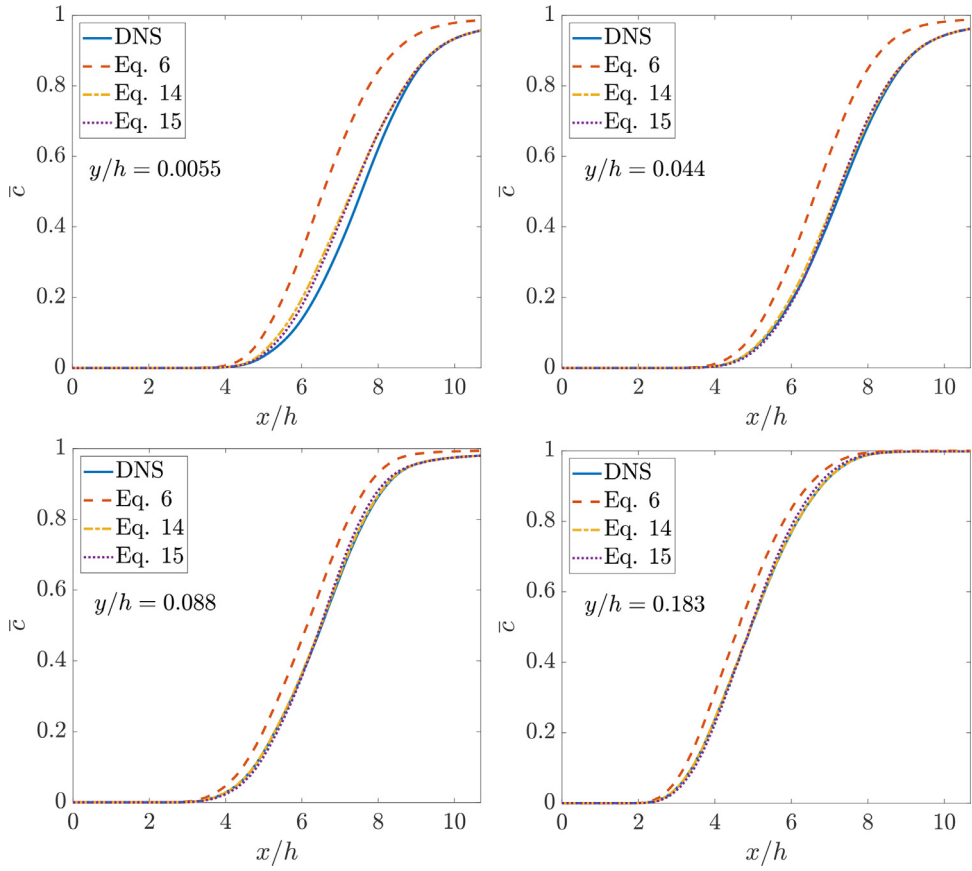


Fig. 13. Reynolds averaged progress variable in case-A compared with different model predictions at different distances away from the wall.

(15) for case-A. Note that in the case of Eq. (15) the value of $Le = 1.0$ has been used. The prediction from Eq. (6) tends to deviate from the DNS data in the near wall region and the prediction improves as the distance from the wall increases. By contrast, the predictions from Eqs. (14) and (15) are in excellent agreement with the DNS data away from the wall while the predicted values for \bar{c} tend to deviate from the DNS data in the near wall region. Similar trends are observed in case-B where the predictions from Eq. (6) tend to show some agreement with the DNS data at earlier times when the flame is away from the wall, as shown in Fig. 14. This agreement between the prediction from Eq. (6) and the DNS data deteriorates as the time progresses and the flame starts to interact with the wall. By contrast, the predictions from Eqs. (14) and

(15) show excellent agreement with the DNS data at earlier times when the flame is away from the wall and a slight deviation from the DNS data can be observed in the near wall region at the later stages of FWI.

4.5. Behaviour of the flame orientation factor

Understanding the behaviour of the flame orientation factor σ_y is useful to be able to model Σ_{gen} through the flamelet crossing frequency approach. In the literature σ_y is usually considered to assume a constant value of 0.5 [35,36,45,48,52,54]. Trouvé and

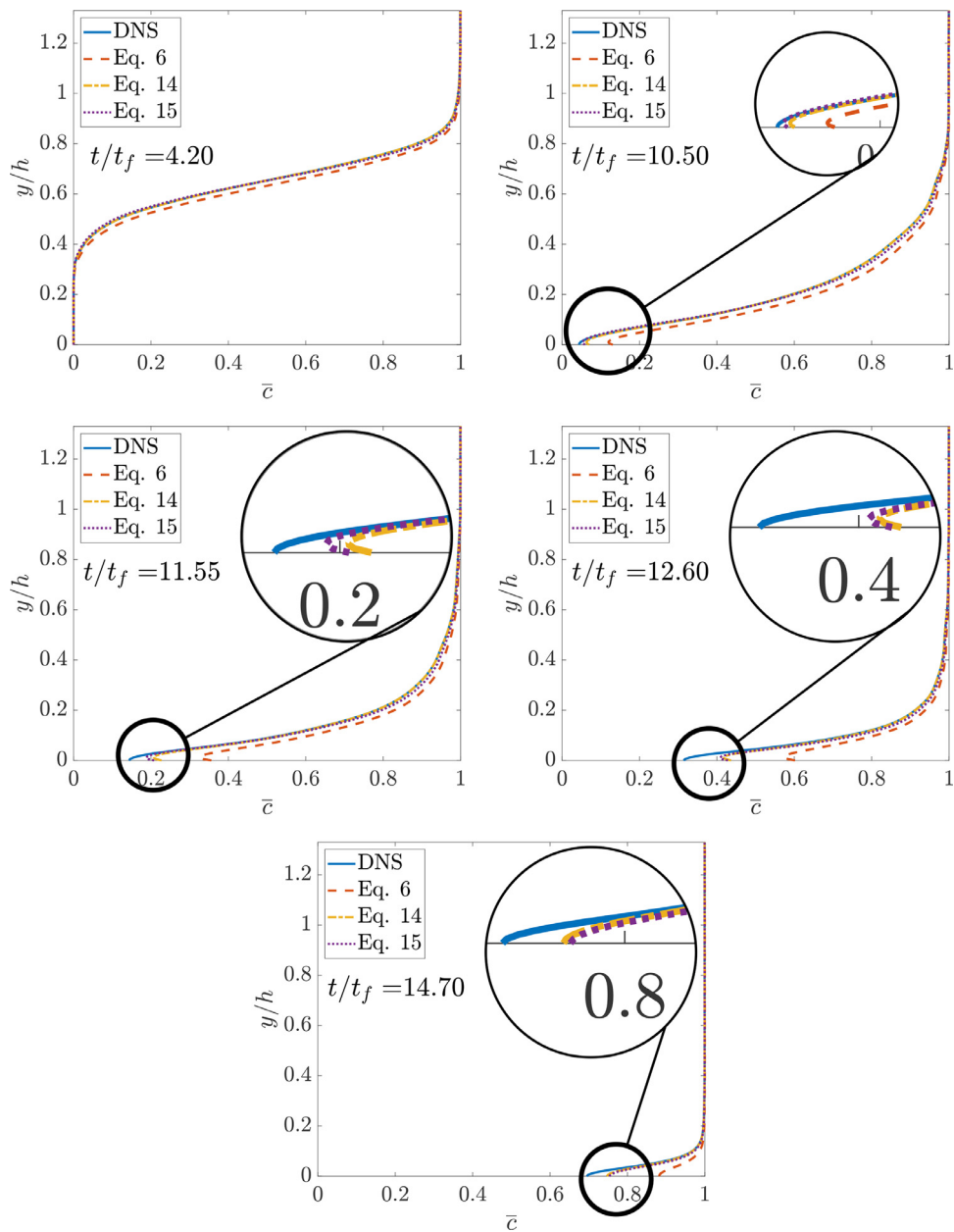


Fig. 14. Reynolds averaged progress variable for case-B compared with different model predictions at different time instants.

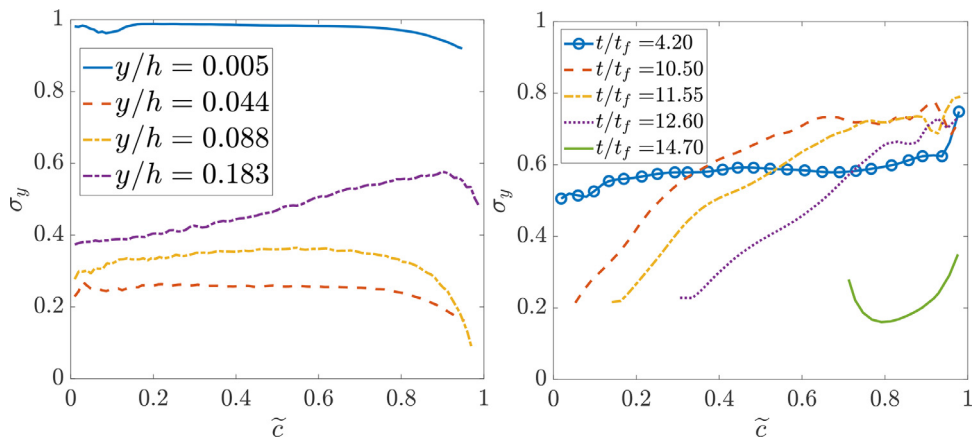


Fig. 15. Variation of σ_y at different locations away from the wall for case-A (left) and at different time instants for case-B (right).

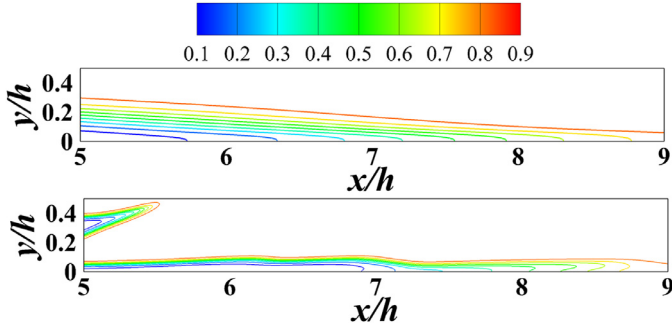


Fig. 16. Behaviour of the Reynolds averaged isosurface of the progress variable (top) and the instantaneous isosurface (bottom) of the progress variable on the x - y mid-plane of the domain in the V-flame case.

Poinsett [71] demonstrated that σ_y can be expressed as:

$$\sigma_y = \sqrt{\left\langle \sqrt{1 - \left(\frac{\nabla c}{|\nabla c|} \cdot \frac{\nabla \bar{c}}{|\nabla \bar{c}|} \right)^2} \right\rangle_s}, \quad (16)$$

where $\langle Q \rangle_s = \overline{Q |\nabla c|} / \Sigma_{gen}$ represents the surface averaged value for a general quantity Q [71]. The expression in Eq. (16) is used to evaluate σ_y from the DNS data. The variations of σ_y for case-A are shown in Fig. 15 at different locations away from the wall. In this case σ_y assumes an almost constant value across the flame and $\sigma_y \approx 0.5$ at $y/h = 0.183$ where the flame is closest to the BML limit. As the distance to the wall decreases the value of σ_y tends to decrease at $y/h = 0.088$ and $y/h = 0.044$ before increasing close to unity in the vicinity of the wall at $y/h = 0.005$. This implies that the instantaneous flamelet normal makes substantial angle with

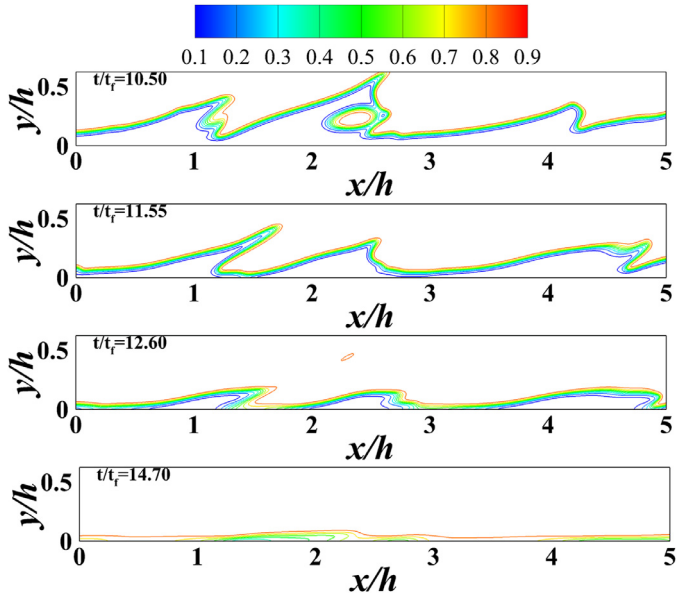


Fig. 17. Behaviour of the instantaneous isosurfaces of the progress variable (between $c = 0.1$ and $c = 0.9$) on the x - y mid-plane of the domain of the head-on quenching planar flame.

the normal vector on the \bar{c} isosurface at $y/h = 0.005$ for case-A. This can be substantiated further by examining the isosurfaces of the instantaneous flame and \bar{c} as shown in Fig. 16 for the Reynolds averaged and instantaneous progress variable. It can be seen that the flame isosurface tends to become stretched in the vicinity of the wall due to the constriction of the scalar gradients in the wall

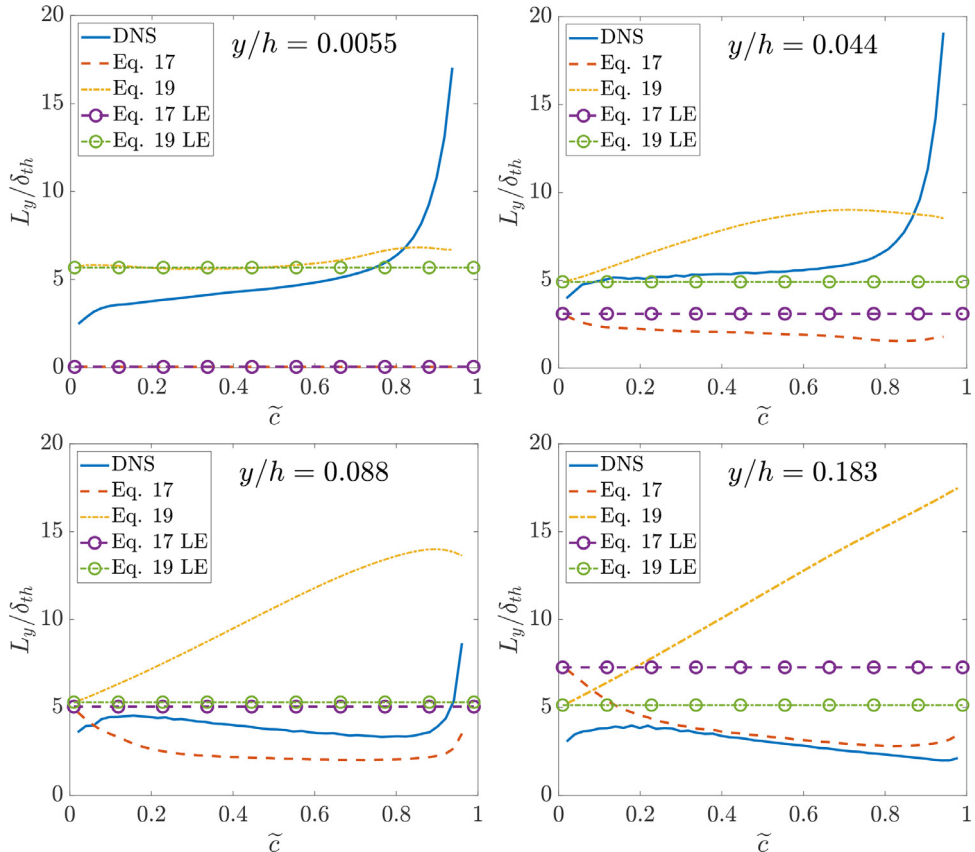


Fig. 18. Flamelet length scale evaluated from the DNS and comparisons with the models for case-A at different distances away from the wall.

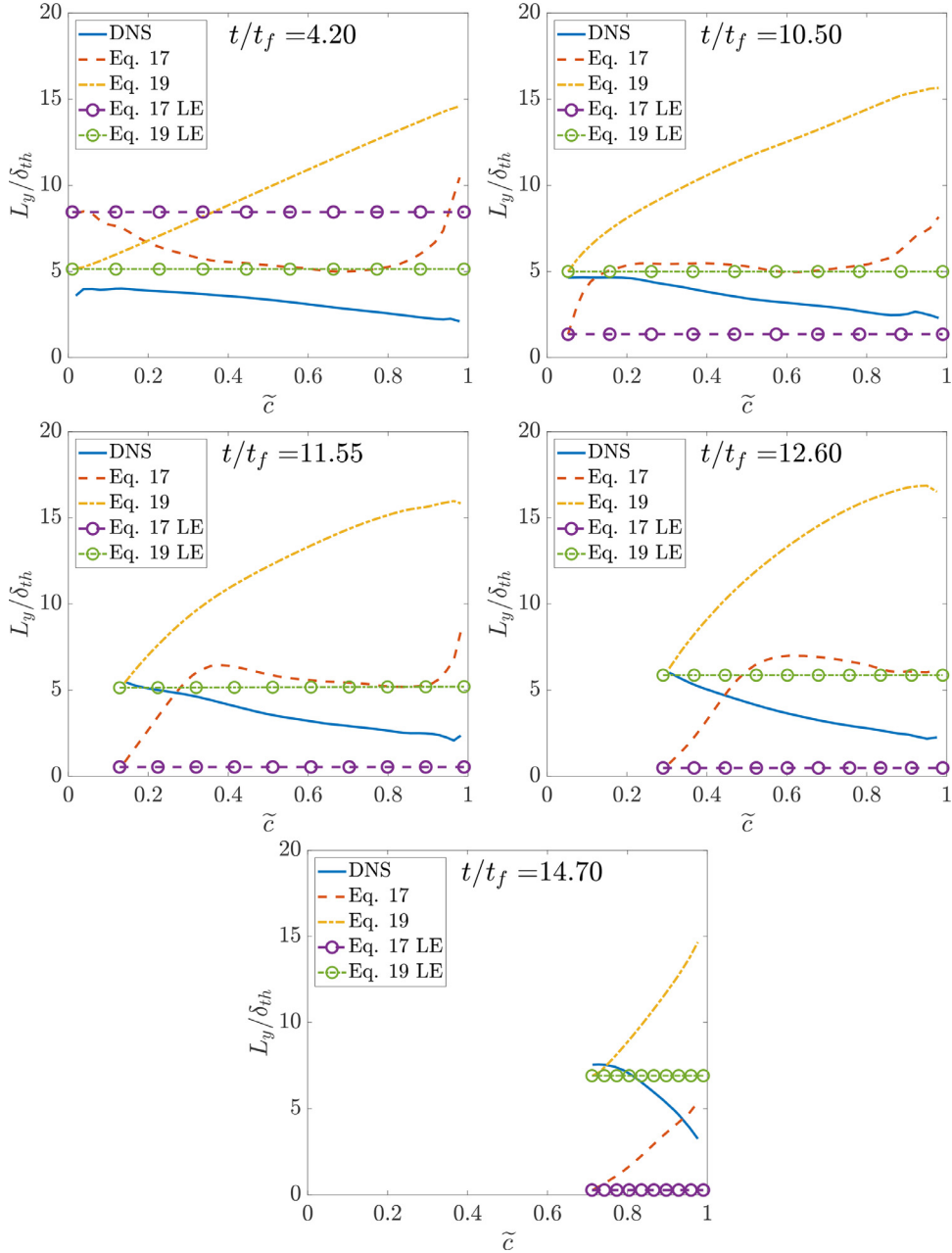


Fig. 19. Flamelet length scale evaluated from the DNS and comparisons with the models for case-B at different time instants.

normal direction and also due to low levels of turbulence leading to the domination of diffusion processes in such a manner that the local flame normal vector remains approximately perpendicular to the normal vectors of \bar{c} isosurfaces which are found to be perpendicular to the wall at very small y/h .

Figure 15 also shows the variation of σ_y at different times for case-B. It can be noticed that $\sigma_y \approx 0.5$ at earlier times when the flame is away from the wall. As the flame starts to interact with the wall the value of σ_y decreases at the leading edge of the flame (i.e. the region of the flame in the vicinity of the cold wall) and increases for the latter part of the flame. This trend continues until $t/t_f = 12.60$ after which the value for σ_y decreases to $\sigma_y \approx 0.2$. These variations in σ_y for case-B arise due to the changes in instantaneous flame surface caused by the wall ejections as the flame enters the turbulent boundary layer. It should be recognised here that this is a statistically 1-D flame and the \bar{c} isosurfaces are parallel to the wall in this flow configuration. During FWI the flame surface

at the leading edge becomes more wrinkled due to wall ejections and the flame normal vector can be locally perpendicular to the wall while the trailing edge remains more parallel to the wall until it starts to interact with the wall ejections in the near wall region at later times. This can be confirmed by examining Fig. 17 which shows the instantaneous c isosurfaces on the $x-y$ mid-plane at different time instants while the flame is interacting with the wall.

Note that the significant differences between the values of σ_y for case-A and case-B during FWI are a result of the orientation of the flame in the near wall region. This is due to the fact that in case-A the flame interacts with the wall in an oblique manner and experiences different fluid mechanical effects when compared with the flame in case-B where the flame interacts with the wall in a head-on manner. For example, the V-flame is a statistically stationary configuration where the supply of the unburned reactants is maintained, whereas the head-on quenching configuration is an unsteady one and the reactants are not replenished during FWI.

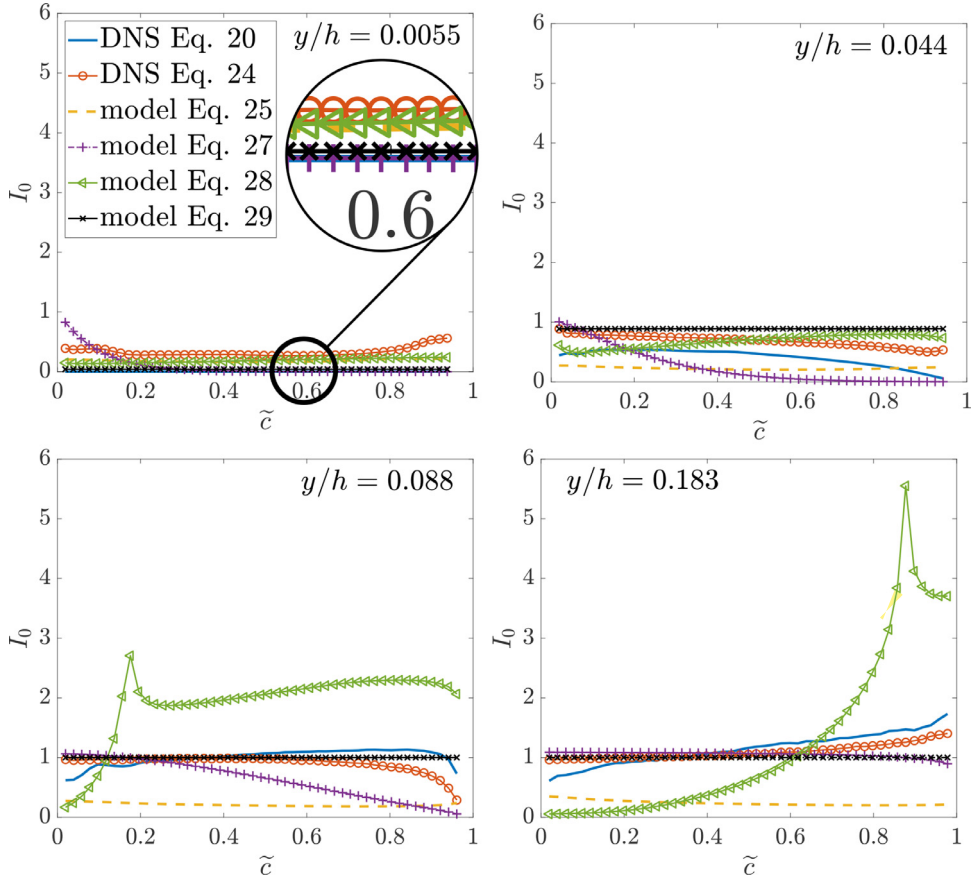


Fig. 20. Stretch factor evaluated from the DNS and comparisons with the models for case-A at different distances away from the wall.

These variations of the flame orientation factor due to the local fluid motion are not only limited to FWI and also exist in laboratory scale flames, as reported in the experimental results of Sattler et al. [72] for an unconfined laboratory scale premixed V-flame.

4.6. Behaviour of the flamelet length scale

The evaluation of the flamelet length scale is necessary to close the generalised FSD Σ_{gen} via the flamelet crossing frequency approach. There are several closures available in the literature for the flamelet length scale. The most commonly used closure is provided by Bray et al. [48] which relates the flamelet length scale to the integral scale of turbulence as:

$$L_y = C_L \left(\frac{\tilde{k}^{3/2}}{\tilde{\epsilon}} \right) \left(\frac{S_L}{\sqrt{2\tilde{k}/3}} \right)^n, \quad (17)$$

where $C_L = 1$, $n = 1$ and \tilde{k} and $\tilde{\epsilon}$ are the Favre averaged turbulent kinetic energy and its dissipation rate, respectively, defined as:

$$\tilde{k} = \frac{\rho u''_k u''_k}{\bar{\rho}} \quad \text{and} \quad \tilde{\epsilon} = \mu \left(\frac{\partial u''_i}{\partial x_k} \frac{\partial u''_i}{\partial x_k} \right) / \bar{\rho}. \quad (18)$$

Abu-Orf and Cant [45] have proposed an expression for L_y which includes modifications to the time scales such that the high reaction rate predictions in the near wall regions from flamelet models can be avoided. The modified expression for L_y reads [45]:

$$L_y = C'_L \left(\frac{\nu}{S_L} \right) \left[\frac{1}{1 + \frac{C_{W_1} S_L}{\sqrt{2\tilde{k}/3}}} \left(1 - \exp \left(-\frac{1}{1 + C_{W_2} \frac{\sqrt{2\tilde{k}/3}}{S_L}} \right) \right) \right]^{-1},$$

$$(19)$$

where $C'_L = 1.0$, $C_{W_1} = 1.5$ and $C_{W_2} = 4.0$ are the model parameters [45] and ν is the kinematic viscosity.

The variation of L_y from the DNS data can be seen in Fig. 18 for case-A. It can be noticed from Fig. 18 that the magnitude of L_y tends to decrease as the distances from the wall increases, but overall the magnitude of L_y remains of the order of $5\delta_{th}$ within the flame. The model predictions from Eqs. (17) and (19) are also shown in Fig. 18 where "LE" implies the quantities evaluated at the leading edge of the mean flame brush which is obtained by sampling the turbulence quantities at the minimum non-zero value of \tilde{c} at a given y/h location. This is done because most of these models are originally proposed based on the values of turbulence upstream of the flame in the unburned gases. It can be seen in Fig. 18 that the expression in Eq. (19) tends to overpredict the trends for all y/h locations while the expressions in Eq. (17) tends to underpredict the values of L_y across the flame. In the case when the models are used based on the turbulence statistics upstream of the flame in the unburned gases the expression in Eq. (19) tends to provide a better estimate for L_y at all the y/h locations when compared with the predictions from Eq. (17). The predictions from Eq. (17) based on the leading edge turbulence statistics improve as the distance from the wall increases.

Figure 19 shows the variation of L_y and the model predictions from Eqs. (17) and (19) at different time instances for case-B. It can be seen from Fig. 19 that all the models either tend to under- or overpredict the values of L_y at all time instances. Similar to case-A the models have also been evaluated using the leading edge turbulence statistics represented by "LE". In this case the leading edge is identified in the same way as done for case-A, but instead of sampling data for a unique y/h , the data is sampled for a unique

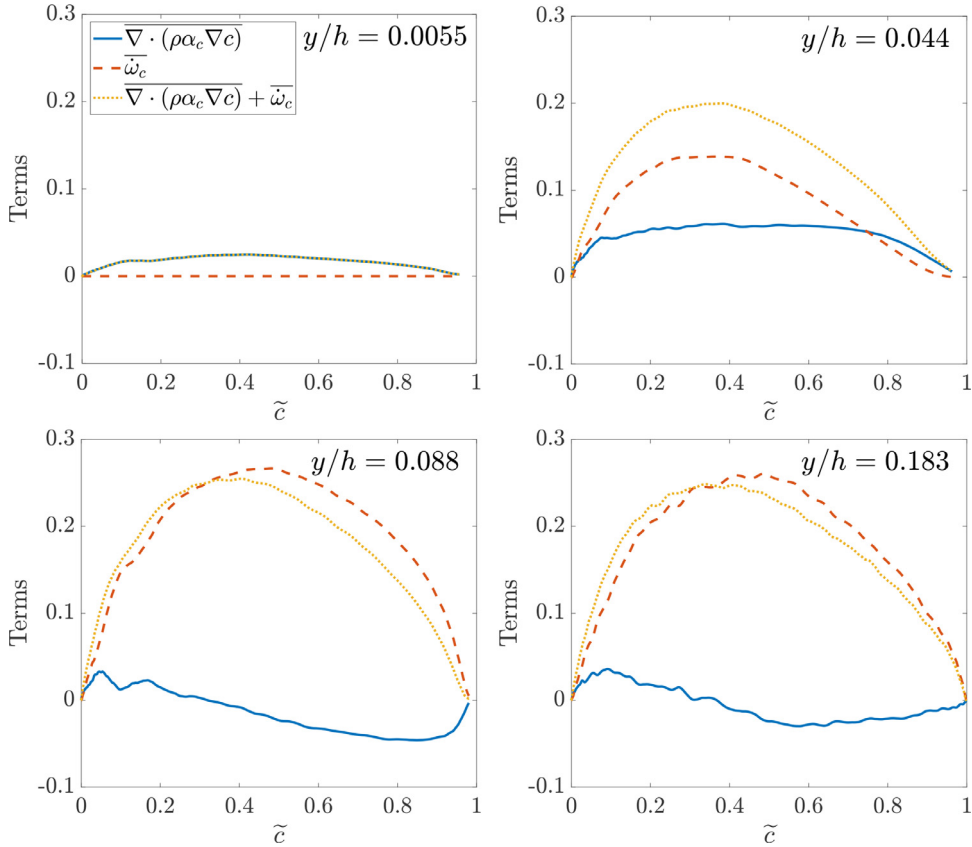


Fig. 21. Variation of $\bar{\omega}_c$, $\nabla \cdot (\rho \alpha_c \nabla c)$ and $\bar{\omega}_c + \nabla \cdot (\rho \alpha_c \nabla c)$ evaluated from the DNS for case-A at different distances away from the wall. The values are normalised using the respective ρ_R , S_L and δ_{th} .

t/t_f . It should be noted that the leading edge of the mean flame brush is not in the fully unburned gases in this case during the FWI process, but the changes in the kinematic viscosity do not exist at the wall as the temperature at the wall is the same as the unburned gas temperature, so the turbulence statistics adjacent to the wall are not significantly altered by the changes in the kinematic viscosity. Note that the predictions from Eq. (19) based on the leading edge of the flame provide the best agreement with L_y obtained from the DNS data, but there is scope for an improvement to the models for L_y to obtain an accurate prediction of the flamelet length scale in FWI of premixed flames in turbulent boundary layers.

4.7. Behaviour of the stretch factor

The statistical behaviour of the stretch factor I_0 is important from the point of view of closing the mean reaction rate as shown in Eq. (9) and can be evaluated as:

$$I_0 = \frac{\bar{\omega}_c}{\rho_R S_L \Sigma_{gen}}. \quad (20)$$

Another way of evaluating I_0 is to define it in terms of the surface averaged displacement speed following the argument that the first two terms on the right hand side of Eq. (2) can be approximated as [47]:

$$\bar{\omega}_c + \frac{\partial}{\partial x_j} \left(\rho \alpha_c \frac{\partial c}{\partial x_j} \right) = \langle \rho S_d \rangle_s \Sigma_{gen}, \quad (21)$$

where S_d is the displacement speed defined as [73]:

$$S_d = \frac{\dot{\omega}_c + \nabla \cdot (\rho \alpha_c \nabla c)}{\rho |\nabla c|}. \quad (22)$$

In the RANS framework, the magnitude of the diffusion term is assumed to be negligible when compared with the mean reaction rate (i.e. $\dot{\omega}_c \gg |\nabla \cdot (\rho \alpha_c \nabla c)|$) which leads to the following expression [47]:

$$\bar{\omega}_c \approx \langle \rho S_d \rangle_s \Sigma_{gen} = I_0 \rho_R S_L \Sigma_{gen}. \quad (23)$$

Consequently the stretch factor can be evaluated as:

$$I_0 = \frac{\langle \rho S_d \rangle_s}{\rho_R S_L}. \quad (24)$$

Bray [52] using data from Abdel-Gayed et al. [74] proposed a modelled expression for I_0 as:

$$I_0 = \frac{0.117 K a_L^{-0.784}}{(1 + \tau)}, \quad (25)$$

where $K a_L$ is the local Karlovitz number defined as :

$$K a_L = 0.157 \left(\frac{\sqrt{2k/3}}{S_L} \right)^2 \left(\frac{\sqrt{2/3} \rho_R \tilde{k}^2}{\mu_R \tilde{\epsilon}} \right)^{-0.5}. \quad (26)$$

In the case of FWI an expression for I_0 has been proposed by Bruneaux et al. [12]:

$$I_0 = \exp[-\gamma_Q \beta_z L_H], \quad (27)$$

where $\gamma_Q = 2$ and $L_H = (\tilde{c} - \tilde{T})$. In other FWI models, I_0 is assumed to be unity when closing the mean reaction rate via Eq. (8), but a modification is introduced in the modelled expression for Σ_{gen} [2,10]. This modification can be taken to be equal to I_0 and consequently a modelled expression for I_0 can be obtained from the modelled expressions of Σ_{gen} . The model proposed by Alshaalan

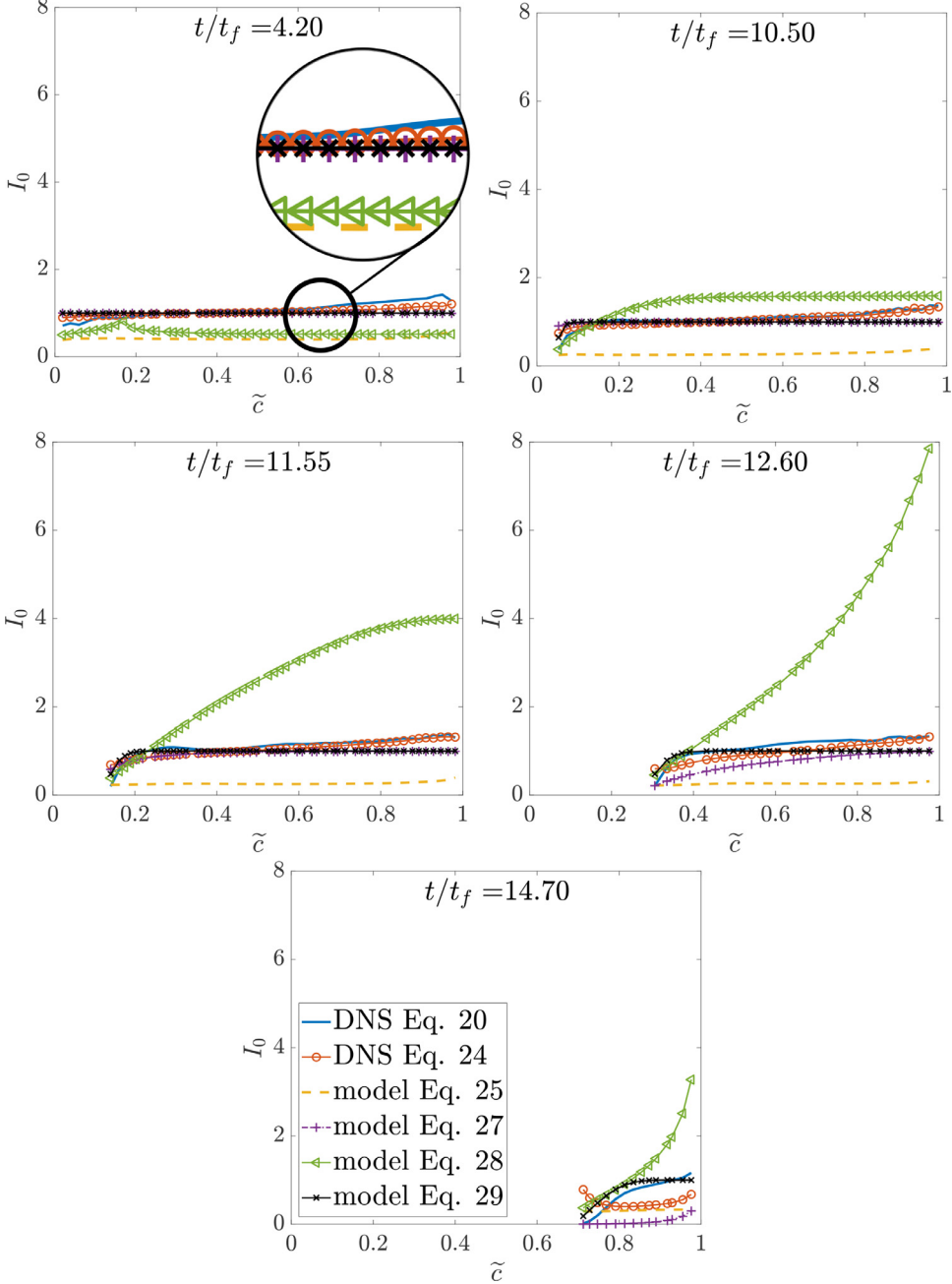


Fig. 22. Stretch factor evaluated from the DNS and comparisons with the models for case-B at different time instants.

and Rutland [2] for Σ_{gen} leads to the following expression :

$$I_0 = (1 + c_y \tilde{A}_w) \exp \left[-\beta_z \left(\frac{\tau \tilde{A}}{(1 + \tau \tilde{T})(1 + \tau \tilde{c})} \right)^{c_x} \right], \quad (28)$$

where $\tilde{A} = (\tilde{c} - \tilde{T})$, $c_y = 48$ and $c_x = 0.25$. The subscript w implies the values at the wall. Similarly, a model for I_0 can be obtained from the modelled expression for Σ_{gen} proposed by Sellmann et al. [10] and in the case of $Le = 1$ can be expressed as :

$$I_0 = 0.5 \left[\operatorname{erf} \left(\frac{y}{\delta_z} - 0.7 Pe_{Q_L} \right) + 1 \right], \quad (29)$$

where y is the distance in the wall normal direction and Pe_{Q_L} is the minimum Peclet number in the case of a conventional 1-D laminar head-on quenching flame.

Figure 20 shows the variations of I_0 for case-A at different distances away from the wall. The value of I_0 is of the order of 1.0 in the regions of the flame away from the wall, as evaluated by using Eqs. (20) and (24). However, I_0 decreases in the near wall region and attains a value of $I_0 \approx 0$ at $y/h = 0.0055$ as estimated by Eq. (20), while $I_0 \approx 0.5$ as estimated by Eq. (24). The values of I_0 away from the wall at $y/h = 0.183$ are consistent with the values reported in the literature [75] and it should be recognised here that the assumption to ignore the effects of molecular diffusion are not valid in Eq. (20) for the near wall region. This can be substantiated by investigating the behaviour of $\dot{\omega}_c$ and $\nabla \cdot (\rho \alpha_c \nabla c)$ and their respective sum, as shown in Fig. 21. Note that the mean molecular diffusion magnitudes are much smaller than the mean reaction rate at $y/h = 0.183$ but the relative magnitudes of the mean molecular diffusion rate in comparison to the mean reaction rate progressively increase and start to dominate in the vicinity of the

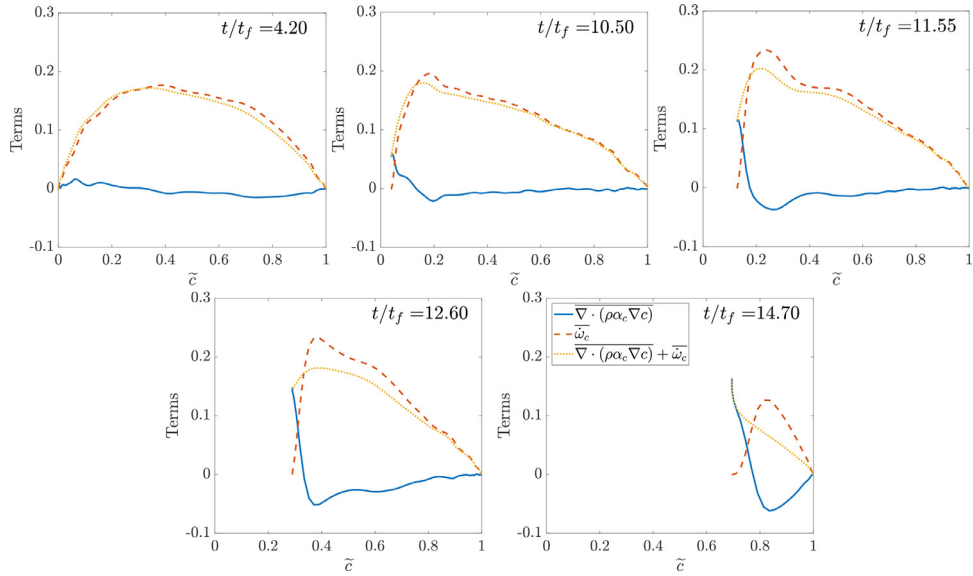


Fig. 23. Variation of $\overline{\omega}_c$, $\overline{\nabla} \cdot (\rho\alpha_c \nabla c)$ and $\overline{\omega}_c + \overline{\nabla} \cdot (\rho\alpha_c \nabla c)$ evaluated from the DNS for case-B at different time instants. The values are normalised using the respective ρ_R , S_L and δ_{th} .

wall at $y/h = 0.005$. As the expression for I_0 in Eq. (24) accounts for these effects, the definition of I_0 based on Eq. (24) is utilised for the discussion of the results obtained from the modelled predictions. The modelled predictions from Eq. (25) are also shown in Fig. 20 and it can be seen that the model in Eq. 25 predicts an almost constant I_0 value across the flame and at all distances away from the wall. By contrast, the expressions in Eqs. (27) and (29) are able to predict the correct order of magnitude for I_0 when the flame is away from the wall and the predictions deteriorate as the wall is approached, as shown in Fig. 20. Figure 20 also shows that the expression in Eq. (28) provides a reasonable prediction in an order of magnitude sense in the near wall region and the performance deteriorates as the distance from the wall increases.

Figure 22 shows the distribution of I_0 in case-B at different time instants using expressions in both Eqs. (20) and (24). At the earlier times in case-B when the flame is away from the wall the value of $I_0 \approx 1$ and similar trends are observed from Eqs. (20) and (24). When the leading edge of the flame brush starts interacting with the wall the value of I_0 evaluated from Eqs. (20) and (24) drops locally at the leading edge while $I_0 \approx 1$ is retained in the rest of the flame brush up to $t/t_f = 12.60$. Some local differences in the values evaluated from Eqs. (20) and (24) can be seen at the leading edge of the flame when it is interacting with the isothermal wall. At $t/t_f = 14.70$ a significant variation in the evaluated values from Eqs. (20) and (24) can be observed and these variations are due to the non-negligible mean molecular diffusion rate magnitudes as shown in Fig. 23. It is evident from Fig. 23 that the mean molecular diffusion rate cannot be ignored in the near wall region and these effects are independent of the flame configuration in FWI. Similar to case-A, the definition of I_0 based on Eq. (24) is utilised for the discussion of the results obtained from the modelled predictions. In case-B the modelled expression in Eq. (25) tends to behave similar to that in case-A and predicts a constant value across the flame for all the time instants. The expressions in Eqs. (27) and (29) tend to predict the correct trends and magnitude for I_0 at earlier times (i.e. when the flame is away from the wall). However, the modelled expression in Eq. (28) provides an underestimated value of I_0 and its performance deteriorates as time progresses and the flame interacts with the wall (i.e. $t/t_f > 4.20$). This aforementioned behaviour of the models in both cases implies that the models in Eqs. (27) and (29) provide the best overall quantitative agreement

amongst the existing models for I_0 , but modifications to the models for I_0 are needed to account for the turbulent boundary layer to be able to accurately predict the flame stretch factor in wall bounded reacting flows.

5. Summary and conclusions

Direct numerical simulations (DNS) for two different turbulent flames interacting with chemically inert isothermal walls at the unburned gas temperature in fully developed turbulent boundary layers have been performed at a friction velocity based Reynolds number of $Re_\tau = 110$. The main differences in the two flames originate from the flow configuration and the flame orientation with respect to the wall. The first configuration is representative of oblique flame-wall interaction (FWI) within a turbulent channel flow, while the second configuration is head-on quenching of a planar flame in a turbulent boundary layer. Mean quantities such as density, axial velocity, temperature and progress variable have been investigated for both cases and it is found that the flame brush thickens during the FWI process in both cases. This variation in the flame thickness implies changes in the flame behaviour and deviations from the strict flamelet limit. In this spirit the applicability of the Bray Moss Libby (BML) formulation is assessed for the two flow configurations which are representative of the corrugated flamelets regime when the flame is away from the wall. It is found that in both cases the probability density function (PDF) of the reaction progress variable c is bi-modal when the flame is away from the wall while the PDF shape changes in the vicinity of the wall and this change in shape is dependent on the flow configuration and the flame orientation with respect to the wall. In the case of oblique FWI in the vicinity of the wall, the PDF of c is found to be mono-modal at the leading and trailing edges of the flame and shows a beta function type behaviour in the interior of the flame. In the case of head-on quenching, the PDF of c remains bi-modal for a longer time and becomes mono-modal at the trailing edge of the flame at the later stages of FWI. Several closures from the BML formulation including the variance of the progress variable c'^2 and the Reynolds averaged progress variable \bar{c} have also been investigated. It is found that the flame configuration in turbulent boundary layers plays a significant role in the behaviour of the aforementioned quantities when the flame interacts with the

wall. The values for \bar{c} in the case of head-on quenching start to vanish when the flame is interacting with the wall, whereas in the case of oblique FWI the full range of \bar{c} is available. Furthermore, in the case of oblique FWI the value of c'^2 decreases rapidly as the flame approaches the wall while in the case of head-on quenching c'^2 only decreases when the flame is close to quenching. These differences between the two configurations exist due to the fact that there is a constant supply of reactants in the case of oblique FWI while in the case of head-on quenching the flame quenches not only due to the cold wall but also due to the consumption of the reactants within the domain. It is also found that closures for \bar{c} and c'^2 in the literature need to be revised for the prediction of FWI events in turbulent boundary layers. Furthermore, the quantities needed for the associated mean reaction rate closure including the flame orientation factor σ_y , flamelet length scale L_y and the flame stretch factor I_0 have also been evaluated from the DNS data for the two flame configurations and the corresponding results are also compared with the closures for these quantities proposed in the literature. It is found that σ_y varies significantly for both cases due to the variation in the flow configuration and the existing closures for L_y and I_0 need improvement to enable satisfactory quantitative predictions of these quantities during the FWI process within turbulent boundary layers. It is also found that the model performance for L_y improves if the statistics for turbulence at the leading edge are used as input parameters to the models. Under these conditions the model proposed by Aby-Orf and Cant [45] provides the best quantitative agreement in the order of magnitude sense for L_y . The investigation for I_0 has revealed that the models proposed by Sellmann et al. [10] for head-on quenching under decaying isotropic turbulence works well for the two FWI flow configurations with fully developed turbulent boundary layers considered in this work. It is also recognised in this work that the magnitude of the mean molecular diffusion rate $\nabla \cdot (\rho \alpha_c \nabla c)$ cannot be ignored in comparison to the mean reaction rate $\dot{\omega}_c$ in the near wall region and should be included in the modelling approach. It should be recognised here that the effects due to the variation of Lewis number, variations in the wall temperature and high Reynolds number will play a role in determining the statistics during FWI. These aspects along with the investigation of detailed chemistry FWI in fully developed boundary layers will form part of the future investigations.

Declaration of Competing Interest

The authors declare that they have no known competing financial interests or personal relationships that could have appeared to influence the work reported in this paper.

Acknowledgments

The authors are grateful for the financial support from the Engineering and Physical Sciences Research Council (Grant: EP/P022286/1). The computational support was provided by ARCHER (EP/K025163/1, EP/R029369/1), CIRRUS, SuperMUC-NG via Leibniz Supercomputing Centre (Grant: pn69ga, pn34xu), and ROCKET (HPC facility at Newcastle University).

References

- [1] T.M. Alshaalan, C.J. Rutland, Wall heat flux in turbulent premixed reacting flow, Combust. Sci. Technol. 174 (2002) 135–165.
- [2] T.M. Alshaalan, C.J. Rutland, Turbulence, scalar transport, and reaction rates in flame-wall interaction, Symp. (Int.) Combust. 27 (1998) 793–799.
- [3] T.J. Poinsot, D. Haworth, G. Bruneaux, Direct simulation and modeling of flame-wall interaction for premixed turbulent combustion, Combust. Flame 95 (1993) 118–132.
- [4] U. Ahmed, N.A.K. Doan, J. Lai, M. Klein, N. Chakraborty, N. Swaminathan, Multiscale analysis of head-on quenching premixed turbulent flames, Phys. Fluids 30 (2018) 105102.
- [5] J. Lai, N. Chakraborty, A priori direct numerical simulation modeling of scalar dissipation rate transport in head-on quenching of turbulent premixed flames, Combust. Sci. Technol. 188 (2016a) 1440–1471.
- [6] J. Lai, N. Chakraborty, Effects of lewis number on head on quenching of turbulent premixed flames: a direct numerical simulation analysis, Flow Turbul. Combust. 96 (2016b) 279–308.
- [7] J. Lai, N. Chakraborty, A.N. Lipatnikov, Statistical behaviour of vorticity and enstrophy transport in head-on quenching of turbulent premixed flames, Eur. J. Mech. B/Fluids 65 (2017) 384–397.
- [8] J. Lai, M. Klein, N. Chakraborty, Direct numerical simulation of head-on quenching of statistically planar turbulent premixed methane-air flames using a detailed chemical mechanism, Flow Turbul. Combust. 101 (2018a) 1073–1091.
- [9] J. Lai, D.H. Wacks, N. Chakraborty, Flow topology distribution in head-on quenching of turbulent premixed flame: a direct numerical simulation analysis, Fuel 224 (2018b) 186–209.
- [10] J. Sellmann, J. Lai, A.M. Kempf, N. Chakraborty, Flame surface density based modelling of head-on quenching of turbulent premixed flames, Proc. Combust. Inst. 36 (2017) 1817–1825.
- [11] G. Bruneaux, K. Akselvoll, T.J. Poinsot, J.H. Ferziger, Flame-wall interaction simulation in a turbulent channel flow, Combust. Flame 107 (1996) 27–36.
- [12] G. Bruneaux, T.J. Poinsot, J.H. Ferziger, Premixed flame-wall interaction in a turbulent channel flow: budget for the flame surface density evolution equation and modelling, J. Fluid Mech. 349 (1997) 191–219.
- [13] A. Gruber, R. Sankaran, E.R. Hawkes, J.H. Chen, Turbulent flame-wall interaction: a direct numerical simulation study, J. Fluid Mech. 658 (2010) 5–32.
- [14] U. Ahmed, N. Chakraborty, M. Klein, Scalar gradient and strain rate statistics in oblique premixed flame-wall interaction within turbulent channel flows, Flow Turbul. Combust. 106 (2021) 701–732.
- [15] A. Gruber, J.H. Chen, D. Valiev, C.K. Law, Direct numerical simulation of premixed flame boundary layer flashback in turbulent channel flow, J. Fluid Mech. 709 (2012) 516–542.
- [16] A. Gruber, E.S. Richardson, K. Aditya, J.H. Chen, Direct numerical simulations of premixed and stratified flame propagation in turbulent channel flow, Phys. Rev. Fluids 3 (2018) 110507.
- [17] T. Kitano, T. Tsuji, R. Kurose, S. Komori, Effect of pressure oscillations on flashback characteristics in a turbulent channel flow, Energy Fuels 29 (2015) 6815–6822.
- [18] U. Ahmed, A.L. Pillai, N. Chakraborty, R. Kurose, Statistical behavior of turbulent kinetic energy transport in boundary layer flashback of hydrogen-rich premixed combustion, Phys. Rev. Fluids 4 (2019) 103201.
- [19] U. Ahmed, A.L. Pillai, N. Chakraborty, R. Kurose, Surface density function evolution and the influence of strain rates during turbulent boundary layer flashback of hydrogen-rich premixed combustion, Phys. Fluids 32 (2020) 055112.
- [20] P. Zhao, L. Wang, N. Chakraborty, Analysis of the flame wall interaction in premixed turbulent combustion, J. Fluid Mech. 848 (2018a) 193–218.
- [21] P. Zhao, L. Wang, N. Chakraborty, Strain rate and flame orientation statistics in the near-wall region for turbulent flame-wall interaction, Combust. Theor. Model. 22 (2018b) 921–938.
- [22] P. Zhao, L. Wang, N. Chakraborty, Vectorial structure of the near-wall premixed flame, Phys. Rev. Fluids 4 (2019) 1–16.
- [23] I. Konstantinou, U. Ahmed, N. Chakraborty, Effects of fuel lewis number on the near-wall dynamics for statistically planar turbulent premixed flames impinging on inert cold walls, Combust. Sci. Technol. 193 (2021) 235–265.
- [24] C. Jainski, M. Rißmann, B. Böhm, A. Dreizler, Experimental investigation of flame surface density and mean reaction rate during flame-wall interaction, Proc. Combust. Inst. 36 (2017a) 1827–1834.
- [25] C. Jainski, M. Rißmann, B. Böhm, J. Janicka, A. Dreizler, Sidewall quenching of atmospheric laminar premixed flames studied by laser-based diagnostics, Combust. Flame 183 (2017b) 271–282.
- [26] C. Jainski, M. Rißmann, S. Jakirlic, B. Böhm, A. Dreizler, Quenching of premixed flames at cold walls: effects on the local flow field, Flow Turbul. Combust. 100 (2018) 177–196.
- [27] M. Rißmann, C. Jainski, M. Mann, A. Dreizler, Flame-flow interaction in premixed turbulent flames during transient head-on quenching, Flow Turbul. Combust. 98 (2017) 1025–1038.
- [28] D. Haworth, Progress in probability density function methods for turbulent reacting flows, Prog. Energy Combust. Sci. 36 (2010) 168–259.
- [29] S.B. Pope, PDF Methods for turbulent reactive flows, Prog. Energy Combust. Sci. 11 (1985) 119–192.
- [30] K.N.C. Bray, P.A. Libby, Interaction effects in turbulent premixed flames, Phys. Fluids 19 (1976) 1687.
- [31] K.N.C. Bray, J. Moss, A unified statistical model of the premixed turbulent flame, Acta Astronaut. 4 (1977) 291–319.
- [32] D.B. Spalding, Mixing and chemical reaction in steady confined turbulent flames, Symp. (Int.) Combust. 13 (1971) 649–657.
- [33] D. Bradley, P.H. Gaskell, X.J. Gu, Application of a Reynolds stress, stretched flamelet, mathematical model to computations of turbulent burning velocities and comparison with experiments, Combust. Flame 96 (1994) 221–248.
- [34] K.N.C. Bray, P.A. Libby, J. Moss, Unified modeling approach for premixed turbulent combustion-part i: general formulation, Combust. Flame 61 (1985) 87–102.
- [35] K.N.C. Bray, J. Moss, Flamelet crossing frequencies and mean reaction rates in premixed turbulent combustion, Combust. Sci. Technol. 41 (1984) 143–172.
- [36] K.N.C. Bray, P.A. Libby, Passage times and flamelet crossing frequencies in premixed turbulent combustion, Combust. Sci. Technol. 47 (1986) 253–274.
- [37] U. Ahmed, R. Prosser, A posteriori assessment of algebraic scalar dissipation

- models for RANS simulation of premixed turbulent combustion, *Flow Turbul. Combust.* 100 (2018) 39–73.
- [38] U. Ahmed, R. Prosser, Modelling flame turbulence interaction in RANS simulation of premixed turbulent combustion, *Combust. Theor. Model.* 20 (2016) 34–57.
- [39] P. Bailly, M. Champion, D. Garréton, Counter-gradient diffusion in a confined turbulent premixed flame, *Phys. Fluids* 9 (1997) 766–775.
- [40] R. Prasad, J. Gore, An evaluation of flame surface density models for turbulent premixed jet flames, *Combust. Flame* 116 (1999) 1–14.
- [41] P. Bailly, D. Garréton, O. Simonin, P. Bruel, M. Champion, B. Deshaires, S. Duplantier, S. Sanquer, Experimental and numerical study of a premixed flame stabilized by a rectangular section cylinder, *Symp. (Int.) Combust.* 26 (1996) 923–929.
- [42] S.J. Brookes, R.S. Cant, I.D. Dupere, A.P. Dowling, Computational modelling of self-excited combustion instabilities, *J. Eng. Gas Turbine Power* 123 (2001) 322–326.
- [43] C.A. Armitage, R. Balachandran, E. Mastorakos, R.S. Cant, Investigation of the nonlinear response of turbulent premixed flames to imposed inlet velocity oscillations, *Combust. Flame* 146 (2006) 419–436.
- [44] A.S. Wu, K.N.C. Bray, Application of a coherent flame model to premixed turbulent combustion impinging on a wall, *Combust. Sci. Technol.* 113 (1996) 367–392.
- [45] G.M. Abu-Orf, R.S. Cant, A turbulent reaction rate model for premixed turbulent combustion in spark-ignition engines, *Combust. Flame* 122 (2000) 233–252.
- [46] R.S. Cant, E. Mastorakos, An introduction to turbulent reacting flows, Imperial College Press (2008).
- [47] M. Boger, D. Veynante, H. Boughanem, A. Trouv  , Direct numerical simulation analysis of flame surface density concept for large eddy simulation of turbulent premixed combustion, *Symp. (Int.) Combust.* 27 (1998) 917–925.
- [48] K.N.C. Bray, M. Champion, P.A. Libby, in: R. Borghi, S.N.B. Murthy (Eds.), *Turbulent reactive flows*, Springer US, New York, NY (1989), pp. 541–563.
- [49] S.B. Pope, Computations of turbulent combustion: progress and challenges, *Symp. (Int.) Combust.* 23 (1991) 591–612.
- [50] S. Candel, D. Veynante, F. Laca  , E. Maistre, N. Darabchia, T. Poinsot, in: B. Larrouetou (Ed.), *Recent advances in combustion modelling*, World Scientific, Singapore (1990), pp. 19–64.
- [51] F.E. Marble, J.E. Broadwell, 1977, The coherent flame model for turbulent chemical reactions, Technical Report, Purdue University, TRW-29314-6001-RU-00. Project SQUID.
- [52] K.N.C. Bray, Studies of the turbulent burning velocity, *Proc. R. Soc. Lond. Ser. A Math. Phys. Sci.* 431 (1990) 315–335.
- [53] R.S. Cant, K.N.C. Bray, Strained laminar flamelet calculations of premixed turbulent combustion in a closed vessel, *Symp. (Int.) Combust.* 22 (1989a) 791–799.
- [54] R.S. Cant, K.N.C. Bray, A theoretical model of premixed turbulent combustion in closed vessels, *Combust. Flame* 76 (1989b) 243–263.
- [55] K. Jenkins, R. Cant, D. Knight, L. Sakell, Recent advances in DNS and LES, Second AFOSR Conference at Rutgers - The State University of New Jersey, New Brunswick, USA, Kluwer, Dordrecht (1999), pp. 191–202.
- [56] J. Jarosinski, A survey of recent studies on flame extinction, *Prog Energy Combust. Sci.* 12 (1986) 81–116.
- [57] S. Vosen, R. Greif, C.K. Westbrook, Unsteady heat transfer during laminar flame quenching, *Proc. Combust. Inst.* 20 (1985) 75–83.
- [58] W. Huang, S. Vosen, R. Greif, Heat transfer during laminar flame quenching: effect of fuels, *Proc. Combust. Inst.* 21 (1988) 1853–1860.
- [59] B. Jiang, D. Brouzet, M. Talei, R.L. Gordon, Q. Cazeres, B. Cuenot, Turbulent flame-wall interactions for flames diluted by hot combustion products, *Combust. Flame* 230 (2021) 111432.
- [60] A.J. Aspden, M.S. Day, J.B. Bell, Three-dimensional direct numerical simulation of turbulent lean premixed methane combustion with detailed kinetics, *Combust. Flame* 166 (2016) 266–283.
- [61] T.D. Dunstan, N. Swaminathan, K.N.C. Bray, R.S. Cant, Geometrical properties and turbulent flame speed measurements in stationary premixed v-flames using direct numerical simulation, *Flow Turbul. Combust.* 87 (2010) 237–259.
- [62] T.J. Poinsot, S. Lele, Boundary conditions for direct simulations of compressible viscous flows, *J. Comput. Phys.* 101 (1992) 104–129.
- [63] R.D. Moser, J. Kim, N.N. Mansour, Direct numerical simulation of turbulent channel flow up to $Re\tau=590$, *Phys. Fluids* 11 (1999) 943–945.
- [64] C.S. Yoo, H.G. Im, Characteristic boundary conditions for simulations of compressible reacting flows with multi-dimensional, viscous and reaction effects, *Combust. Theor. Model.* 11 (2007) 259–286.
- [65] T. Tsukahara, Y. Seki, H. Kawamura, D. Tochio, Forth International Symposium on Turbulence and Shear Flow Phenomena, Williamsburg, USA, 935–940.
- [66] J. Lai, A. Moody, N. Chakraborty, Turbulent kinetic energy transport in head-on quenching of turbulent premixed flames in the context of Reynolds averaged Navier stokes simulations, *Fuel* 199 (2017) 456–477.
- [67] U. Ahmed, D.D. Apsley, T. Stallard, P.K. Stansby, I. Afgan, Turbulent length scales and budgets of Reynolds stress-transport for open-channel flows; friction Reynolds numbers $Re\tau = 150, 400$ and 1020, *J. Hydraul. Res.* 59 (2021) 36–50.
- [68] K.N.C. Bray, M. Champion, P.A. Libby, N. Swaminathan, Scalar dissipation and mean reaction rates in premixed turbulent combustion, *Combust. Flame* 158 (2011) 2017–2022.
- [69] H. Kolla, N. Swaminathan, Strained flamelets for turbulent premixed flames II: laboratory flame results, *Combust. Flame* 157 (2010) 1274–1289.
- [70] N. Chakraborty, R.S. Cant, Effects of lewis number on flame surface density transport in turbulent premixed combustion, *Combust. Flame* 158 (2011) 1768–1787.
- [71] A. Trouv  , T.J. Poinsot, The evolution equation for the flame surface density in turbulent premixed combustion, *J. Fluid Mech.* 278 (1994) 1–131.
- [72] S. Sattler, D. Knaus, F. Gouldin, Determination of three-dimensional flamelet orientation distributions in turbulent v-flames from two-dimensional image data, *Proc. Combust. Inst.* 29 (2002) 1785–1792.
- [73] T. Echekki, J.H. Chen, Unsteady strain rate and curvature effects in turbulent premixed methane-air flames, *Combust. Flame* 106 (1996) 184–202.
- [74] R.G. Abdel-Gayed, D. Bradley, A. Lau, The straining of premixed turbulent flames, *Symp. (Int.) Combust.* 22 (1989) 731–738.
- [75] R. Sankaran, E.R. Hawkes, C.S. Yoo, J.H. Chen, Response of flame thickness and propagation speed under intense turbulence in spatially developing lean premixed methane air jet flames, *Combust. Flame* 162 (2015) 3294–3306.